Epstein-Barr virus BNRF1 destabilizes SMC5/6 cohesin complexes to evade its restriction of replication compartments

Stephanie Pei Tung Yiu[1-4], Rui Guo[1,3,4], Cassie Zerbe[5], Michael P. Weekes[5], Benjamin E. Gewurz[1-4,6*]

[1] Division of Infectious Diseases, Department of Medicine, Brigham and Women's Hospital, 181 Longwood Avenue, Boston MA 02115, USA

[2] Harvard Graduate Program in Virology, Boston, MA 02115

[3] Broad Institute of Harvard and MIT, Cambridge, MA 02142, United States of America

[4] Department of Microbiology, Harvard Medical School, Boston, MA 02115, USA

[5] Cambridge Institute for Medical Research, University of Cambridge, Hills Road, Cambridge CB2 0XY, UK

[6] Lead Contact

* Correspondence bgewurz@bwh.harvard.edu

SUMMARY

Epstein-Barr virus (EBV) persistently infects most people worldwide. Delivery of ~170 kilobase EBV genomes to nuclei, and use of nuclear membrane-less replication compartments (RC) for their lytic cycle amplification, necessitate evasion of intrinsic antiviral responses. Proteomic analysis indicates that upon B-cell infection or lytic reactivation, EBV depletes the chromosome maintenance cohesin SMC5/6, which has major chromosome maintenance roles and DNA damage repair. The major tegument protein BNRF1 targets SMC5/6 complexes by a ubiquitin proteasome pathway dependent on calpain proteolysis and cullin-7. In the absence of BNRF1, SMC5/6 associates with R-loop structures, including at the viral lytic origin of replication, and interferes with RC formation and encapsidation. CRISPR analysis identifies RC restriction roles of SMC5/6 components involved in DNA entrapment and SUMOylation. Our studies highlight SMC5/6 as a key intrinsic immune sensor and restriction factor for a human herpesvirus RC and have implications for the pathogenesis of EBV-associated cancers.

Keywords: Structural maintenance of chromosomes, herpesvirus, tegument, lytic reactivation, R-loop, viral replication compartment, innate immunity, antiviral defense, ubiquitin proteasome, calpain

Short Title: EBV BNRF1 prevents SMC5/6 replication compartment restriction

INTRODUCTION

Epstein–Barr virus (EBV) establishes life-long infection in >95% of adults worldwide, is the etiologic agent of infectious mononucleosis, is associated with multiple sclerosis and with ~2% of human cancers (Parkin, 2006; Zur Hausen and de Villiers, 2015). These include endemic Burkitt lymphoma, Hodgkin lymphoma, post-transplant and HIV-associated lymphoma, T and NK-cell lymphomas, nasopharyngeal and gastric carcinomas (Farrell, 2019; Shannon-Lowe et al., 2017). Much remains to be learned about how EBV subverts host immune barriers in order to establish latency, reactivate within the heart of the adaptive immune system and cause cancer.

The Epstein-Barr virion is comprised of a 170 kilobase double stranded DNA (dsDNA) genome packaged in an icosahedral capsid that is surrounded by a proteinaceous tegument and lipid envelope (Rixon and Schmid, 2014). Upon host cell infection, tegument proteins are released, and the EBV capsid traffics to the nuclear pore, where viral genomes are inserted into the nucleus, chromatinized and circularized. EBV tegument protein BNRF1 disrupts ATRX/DAXX complexes to prevent loading of repressive H3.3 histones onto incoming EBV genomes (Tsai et al., 2011). Knowledge remains incomplete about how EBV evades foreign DNA sensors in newly infected cells (Buschle and Hammerschmidt, 2020; Chakravorty et al., 2019; Lieberman, 2013).

Upon EBV lytic reactivation, the immediate early genes BZLF1 (ZTA/Zebra) and BRLF1 (RTA) induce 32 viral early genes that initiate lytic EBV genomes synthesis (Kenney and Mertz, 2014; Miller and El-Guindy, 2002). EBV lytic genes form membrane-less nuclear replication compartments (RC), in which the EBV-encoded polymerase BALF5 produces new genomes., EBV RC occupy nearly 30% of nuclear volume, which itself is doubled upon lytic reactivation (Nagaraju et al., 2019; Speck et al., 1997). The polymerase processivity factor BMRF1 is found exclusively within RC, where hundreds of newly synthesized copies of EBV DNA are organized around BMRF1 cores (Daikoku et al., 2005; Nagaraju et al., 2019; Sugimoto et al., 2013). Whether these structures can be sensed by innate immune sensors is unknown. Two EBV origins of lytic DNA replication (*oriLyt*) serve as key *cis*-acting enhancers of late lytic gene expression (Djavadian et al., 2016; Hammerschmidt and Sugden, 2013). GC-rich regions form RNA: DNA hybrid R loop structures at both *oriLyt* (Rennekamp and Lieberman, 2011).

~30 EBV late genes are transcribed from newly synthesized lytic EBV genomes and encode virion capsid, tegument and glycoproteins. It is not completely understood why EBV late genes requires the production of nascent DNA in RC, though o*riLyt* serves key *cis*-acting enhancer roles

in late gene expression (Djavadian et al., 2016). Ongoing EBV DNA replication maintains RC integrity (Li et al., 2018).

The structural maintenance of chromosomes (SMC) condensin, cohesin and SMC5/6 are ATP-powered, ring-shaped machines that topologically entrap DNA and are major regulators of DNA replication, transcription and chromosome biology (Uhlmann, 2016). Recent studies highlight the capability of SMC5/6 to repress transcription from double stranded DNA viral genomes in the absence of viral evasion mechanisms (Bentley et al., 2018; Decorsiere et al., 2016; Dupont et al., 2021; Gibson and Androphy, 2020; Murphy et al., 2016; Niu et al., 2017; Xu et al., 2018). To avoid silencing, the Hepatitis B virus (HBV) HbX oncoprotein assembles a ubiquitin ligase complex to target SMC6 for proteasomal degradation (Decorsiere et al., 2016; Murphy et al., 2016; Niu et al., 2017). In the absence of HbX, SMC5/6 interacts with the episome to inhibit viral transcription, though the mechanism by which it recognizes viral DNA and alters its expression remain incompletely understood. Similarly, adenovirus-encoded E4 targets SMC5/6 for degradation, in the absence of which, SMC5/6 localizes to viral replication compartments, associates with replicating adenoviral dsDNA genomes and impairs viral lytic DNA replication (Dybas et al., 2021). Much remains to be learned about how SMC5/6 recognizes double stranded viral DNA, and whether it can recognize herpesvirus genomes, including that of EBV in newly infected or lytic cells.

Here, we used recently constructed temporal proteomic maps (Ersing et al., 2017; Wang et al., 2019a) to identify that SMC5/6 is depleted upon primary human EBV B-cell infection and again upon B or epithelial cell EBV lytic reactivation. We identify BNRF1 as necessary and sufficient for SMC5/6 depletion and determine that it mediates SMC5/6 degradation in a calpain, cullin-7 ubiquitin ligase and proteasome dependent manner. In the absence of BNRF1, SMC5/6 interacts with RNA:DNA hybrid R-loop structures, including at o*riLyt* to suppress EBV RC formation, genome encapsidation, sustained late gene expression and infectious virion production. These studies implicate SMC5/6 as a key host restriction factor for a herpesvirus RC.

RESULTS

BNRF1 meditates SMC5/6 complex turnover in EBV B and epithelial cell lytic replication

To identify how EBV lytic replication remodels the B-cell proteome, we recently used whole cell tandem-mass-tag-based analysis to generate unbiased temporal profiles of nearly 8000 host and 69 viral proteins in two Burkitt lymphoma B-cell lines induced for lytic reactivation (Ersing et al., 2017). Interestingly, multiple components of the SMC5/6 complex were rapidly depleted upon EBV lytic reactivation in both P3HR-1 and Akata cells that harbor type I versus II EBV strains, respectively. SMC6 was amongst the most highly depleted human protein within 24 hours of lytic reactivation (Figure 1A-C), raising the question of whether it can restrict EBV lytic replication. EBV is associated with 10% of gastric carcinomas, and we similarly observed that SMC6 abundance was reduced during EBV lytic reactivation in EBV+ AGS gastric carcinoma cells with a doxycycline-inducible immediate early ZTA allele (Verma et al., 2016) (Figure 1D).

We next asked if SMC5/6 complex abundance was perturbed during EBV infection of primary human B-cells, which results in latency as opposed to lytic replication. Using our temporal proteomic map (Wang et al., 2019a), we again found that multiple SMC5/6 cohesin complex subunits were amongst the most highly depleted human proteins at 48 hours post-EBV infection (Figure 1E). Abundances of SMC5, SMC6 and NSE4A cohesin reached a nadir at Day 4 post-infection, a timepoint at which cells begin to rapidly proliferate (Nikitin et al., 2010) (Figure 1F, S1A). Yet, SMC6 mRNA increased over the first 48 hours post-infection, suggesting that changes in its protein abundance likely occurred at the post-transcriptional level. At later timepoints, abundances of SMC5, 6 and NSE4A mRNAs all decreased, perhaps indicative of a second mechanism by which EBV suppresses SMC5/6 following latency establishment (Figure S1A). We validated SMC6 loss at Day 3 post EBV infection of primary and Burkitt B-cells (Figure 1G, S1B-C).

EBV major tegument protein BNRF1 targets SMC5/6 for proteasomal degradation

Proteomic analysis detected multiple EBV capsid, tegument and glycoproteins over the first 96 hours post-infection (hpi), likely delivered by incoming viral particles, as most early gene-products which do not encode virion components were not detected (Wang et al., 2019a). The EBV major tegument protein BNRF1 was amongst the most abundant EBV protein at 48 hpi (Figure 2A), where it was maximally expressed (Figure 2B). To test if BNRF1 was sufficient to mediate SMC6

depletion, a panel of P3HR-1 B-cells were established with conditional HA-epitope tagged EBV lytic protein expression. Doxycycline induction of BNRF1, but not of the other EBV lytic proteins or GFP control, resulted in SMC6 loss (Figure 2C). To avoid possible confounding effects on expression from latent P3HR-1 EBV genomes, EBV- BJAB B-cells with conditional BNRF1 expression were established. BNRF1 expression was sufficient for SMC6 depletion (Figure S2A).

We next asked whether BNRF1 was necessary for SMC6 loss upon EBV lytic reactivation. For this analysis, we used Cas9+ P3HR-1 cells with conditional EBV immediate early protein BZLF1 and BRLF1 alleles fused to a 4-hydroxy tamoxifen (4-HT)-dependent mutant estrogen receptor binding domain (ZHT and RHT, respectively) (Calderwood et al., 2008; Chiu et al., 2013). 4-HT addition causes ZHT/RHT nuclear translocation and EBV lytic reactivation, which is enhanced by the histone deacetylase inhibitor sodium butyrate. To establish CRISPR-edited cells, control or two independent single guide RNAs (sgRNAs) against *BNRF1* were expressed. 4-HT addition induced expression of endogenous immediate early BZLF1 and early BMRF1 genes in control and *BNRF1*-edited cells. However, SMC5/6 depletion was strongly impaired by BNRF1 knockout (KO) (Figure 2D). Levels of the NSE2 and NSE3 SMC5/6 cohesin components were not diminished, indicating that DNA-bound cohesin subunits are preferentially targeted (Figure 1B, 2D).

Rapid SMC5/6 loss raised the possibility that BNRF1 targets the SMC5/6 complex for degradation. In support, immunoblot analysis revealed that SMC6 levels were already strongly reduced by 15hrs post-infection (Figure S2B). Furthermore, the proteasome inhibitor bortezomib or the small molecule neddylation antagonist MLN4924, which blocks activity of cullin-based ubiquitin E3 ligases, each diminished SMC6 depletion upon inducible BNRF1 expression. Co-administration of bortezomib and MLN4924 had additive effects (Figure 2E), indicating that BNRF1 likely utilizes a cullin ubiquitin ligase to target SMC5/6 for proteasomal degradation.

BNRF1 is not known to have ubiquitin ligase activity. Therefore, to gain insights into host proteins used by BNRF1 to deplete SMC5/6, HA-tagged BNRF1, or control EBV tegument proteins BPLF1, BLRF2 and BOLF1, were inducibly expressed and purified by HA-peptide elution from P3HR-1 cells triggered for lytic replication. High confidence BNRF1-selective interactors were identified by liquid chromatography/mass spectrometry analysis of immunopurified material followed by CompPASS analysis (Huttlin et al., 2015). This analysis identified DAXX as a key BNRF1 interactor, in keeping with prior published studies (Huang et al., 2016; Tsai et al., 2011). SMC6 was not detected, perhaps reflecting transient association with BNRF1 in the absence of cullin or proteasome inhibitors. Unexpectedly, multiple calpain subunits were high-confidence

BNRF1 interactors, including the catalytic CAPN1 and regulatory CAPNS1 subunits (Figure 2F, S2C). Calpains are calcium-dependent cysteine proteases that cleave particular protein substrates to facilitate proteolytic processes (Ono and Sorimachi, 2012). We validated that the calpain proteolytic subunit CAPNS1 co-immunoprecipitated with inducibly expressed BNRF1 in bortezomib-treated cells, and also with SMC6 in cells induced for lytic replication (Figure 2G, S2D).

To test whether calpain enzymatic activity was necessary for SMC6 depletion, BNRF1 was induced in the absence or presence of the highly-selective calpain inhibitor calpeptin. A dose-response relationship was observed, and calpeptin rescued SMC6 expression to nearly the same extent as bortezomib/MLN4924 treatment in P3HR-1 cells induced for BNRF1 cDNA expression (Figure 2H). Interestingly, calpain inhibition by *CAPNS1* KO or by calpeptin rescued SMC6 expression upon lytic replication (Figure S2E-F). Calpain inhibition also reduced expression of BNRF1, but not of the early gene BMRF1 (Figure S2E-F). Given that calpeptin did not alter levels of conditionally expressed BNRF1, this result raises the possibility that SMC6 stabilization down-modulates EBV late gene expression.

Calpain proteolysis can generate proteolytic fragments that are then subjected to ubiquitin-dependent degradation by the Arg/N-end rule pathway, which uses cullin E3 ligases (Piatkov et al., 2014; Varshavsky, 2019). We therefore tested whether CRISPR KO of six cullin genes, or the DDB1 adaptor protein of cullin 4A/B complexes, could stabilize SMC6 in P3HR-1 cells induced for lytic replication. Although it has not previously been associated with the N-end rule pathway, Cul7 KO stabilized SMC6 (Figure 2I, S2G). Furthermore, Cul7, but not Cul1, Cul3 or DDB1 co-immunoprecipitated with BNRF1 in lysates from bortezomib-treated P3HR-1 cells induced for lytic replication (Figure S2H). SMC6 complexes immunopurified from whole cell lysates of P3HR-1 induced for lytic replication were highly modified by high molecular weight poly-ubiquitin chains, as judged by immunoblot with the anti-ubiquitin antibody P4D1 (Figure S2I).These data support a model in which BNRF1 drives calpain- and Cul7-dependent SMC6 turnover.

BNRF1 and SMC6 associate at nuclear puncta

BNRF1 binds the histone chaperone DAXX to disrupt ATRX/DAXX complexes and prevent loading of repressive histone 3.3 onto incoming EBV genomes in newly infected cells (Tsai et al., 2011). We asked whether BNRF1 likewise associates with SMC5/6 cohesin complexes by two approaches. First, HA-epitope tagged BNRF1 was inducibly expressed in P3HR-1 cells in the presence of bortezomib, immunopurified and subjected to SDS-PAGE. SMC6 as well as DAXX

co-immunoprecipitated with BNRF1 (Figure 3A). Stably expressed HA-SMC6 reciprocally co-immunoprecipitated endogenous BNRF1 from bortezomib-treated lytic P3HR-1 (Figure S3A). Second, inducibly expressed HA-SMC6 and stably over-expressed V5-BNRF1 co-localized in EBV+ Akata B-cell nuclear puncta in MLN4924 treated cells (Figure 3B). Intriguingly, the subnuclear distribution of stably over-expressed BNRF1 changed substantially in the presence of conditionally expressed SMC6, from a diffuse nuclear pattern to puncta that highly overlapped that of SMC6 (Figure S3B). 3D image reconstruction showed that these puncta were nuclear (Figure S3C-D). Presumably, stable BNRF1 expression achieved levels in excess of endogenous SMC6, and co-expression of HA-SMC6 provided sufficient substrate to re-localize BNRF1 into nuclear SMC6 foci.

BNRF1 residues 300-600 form a globular domain that mediates association histone H3.3/H4-bound DAXX at PML nuclear bodies (Huang et al., 2016; Tsai et al., 2011), leading to disruption of the DAXX/ATRX complex without targeting it for degradation. Since association with BNRF1 instead results in a different fate for the SMC5/6 cohesin complex, we characterized BNRF1 regions that interact with SMC6. BNRF1 wildtype versus internal deletion mutants termed M1-M5 were inducibly expressed in P3HR-1 (Figure 3C). Surprisingly, induction of wildtype (WT), but not deletion mutant BNRF1 caused SMC6 depletion, even though M1-5 were expressed at similar or greater levels than WT BNRF1 (Figure 3D). In agreement with prior studies, co-immunoprecipitation analysis revealed BNRF1 residues 300-600 to be essential for association with DAXX. Yet, each BNRF1 region, particularly M5, was important for association with SMC6 (Figure S3E). Unexpectedly, we found that M2-M5 failed to form nuclear puncta and instead exhibited perinuclear distribution (Figure 3E). These results suggest that multiple BNRF1 regions are likely important for association with SMC6 and localization to nuclear puncta.

Key BNRF1 roles in lytic DNA replication, late gene expression and morphogenesis.

To gain insights into BNRF1 roles in support of lytic replication, we performed RNA-sequencing (RNA-seq) on control versus BNRF1 KO P3HR-1 ZHT/RHT cells, prior to and 24 hours post lytic induction by addition of 4HT and sodium butyrate (NaB). While expression of EBV early lytic genes were somewhat lower in *BNRF1* edited cells, late gene expression was strongly reduced (Figure 4A, S4A), suggesting that BNRF1 may be important for sustaining late gene expression. qPCR analysis of the late lytic genes BVRF1 and BcLF1 validated this result (Figure S4B). To control for CRISPR editing of EBV episome, which is present at higher copy number than host

chromosomes, we used an sgRNA targeting the lytic gene *BXLF1,* which is not essential for EBV replication (Meng et al., 2010). Reduction of EBV late gene gp350 expression was similarly evident on the protein level, where BNRF1 sgRNAs significantly reduced gp350 levels relative to those seen in cells with the control BXLF1 sgRNA (Figures 4B-C). Robust *BXLF1* editing was confirmed by T7E1 assay (Figures S4C). Similar results were observed in EBV+ Akata cells triggered for lytic reactivation by anti-immunoglobulin crosslinking (Figures S4D-F).

As EBV late gene transcription requires continuous lytic DNA replication (Li et al., 2018), we tested if BNRF1 loss affects EBV genome copy number following lytic reactivation. We observed significant reduction in EBV DNA levels in both P3HR-1 and Akata cells expressing independent BNRF1 sgRNAs relative to levels in cells with non-targeting or BXLF1 control sgRNAs (Figure 4D and S4G). This result was unexpected, given only modest effects observed on expression of EBV early genes, which encode factors that replicate viral DNA.

To further characterize BNRF1 KO effects on EBV lytic replication, we utilized transmission electron microscopy (TEM). Intriguingly, TEM demonstrated a significant reduction in nuclear capsids filled with electron dense material characteristic of EBV genomic DNA (Figure 4E-F). ~60% of nuclear capsids lacked electron-dense material in *BNRF1* edited cells, as compared with ~40% in control cells (Figure 4F). Since capsids are encoded by EBV late genes, we suspect that they were synthesized at the onset of the late phase, but that their expression was not sustained at later timepoints, as measured by RNA-seq. Impaired encapsidation may reflect diminished EBV DNA production, a defect in trafficking of DNA to or insertion into viral capsids as a result of diminished late gene expression, or perhaps SMC5/6-mediated EBV lytic DNA compaction.

We next used the green Raji infection assay (Altmann and Hammerschmidt, 2005) to test whether BNRF1 editing reduced titers of EBV released from lytic cells. This assay leverages the GFP marker expressed by EBV bacterial artificial chromosome (BAC) genomes present in producer cells. Super-infection of Raji cells results in a GFP signal. We found that expression of either BNRF1 sgRNA significantly reduced titers of infectious EBV produced by EBV+ Akata cells relative to levels observed in control BXLF1 sgRNA expressing cells (Figure 4G and S4H). Collectively, these results suggest that BNRF1 is important for late lytic cycle progression, viral DNA packaging into nuclear icosahedral capsids, and ultimately secretion of infectious virion.

BNRF1 is critical for EBV replication compartment formation

Ongoing EBV DNA replication is important for maintenance of EBV RC (Li et al., 2018). Since late gene transcription and DNA replication were unexpectedly reduced in *BNRF1*-edited cells, we hypothesized that the SMC5/6 cohesin complex can recognize and restrict EBV RC, thereby serving a key innate immune role. P3HR-1 ZHT/RHT cells induced for lytic replication were treated with the cytosine homologue 5-ethynyl-2'-deoxycytidine (EdC). A click chemistry approach then allowed EdC biotinylation for streptavidin-based visualization (Qu et al., 2011). Since EBV lytic replication causes growth arrest, most EdC incorporation results from EBV lytic DNA incorporation and serves to highlight RC. To further demarcate RC, cells were concurrently immunostained for BMRF1 (Nagaraju et al., 2019). BNRF1 KO by independent sgRNAs, but not control BXLF1 KO, strongly reduced EdC incorporation in P3HR-1 cells induced for lytic replication. Likewise, BNRF1 KO caused striking BMRF1 redistribution, from a globular pattern in control cells to a perinuclear pattern (Figure 5A, S5A). BNRF1 KO did not change overall EdC incorporation (Fig. S5B). 3D image reconstruction showed that globular replication compartment structures were diminished in BNRF1 KO cells (Figure 5B-C, S5C). On-target BNRF1 sgRNA effects on RC formation were confirmed by cDNA rescue, using a BNRF1 construct with silent mutation at the protospacer adjacent motif to abrogate Cas9 cutting (Figure 5D-F, S5D-E).

We reasoned that proteasome inhibition should phenocopy BNRF1 KO effects on the EBV lytic cycle by stabilizing SMC5/6 complexes. Indeed, treatment with 5nM of bortezomib reduced the number of RC formed in P3HR-1 cells by nearly 80% relative to levels in control cells. Since proteasome inhibitors have pleotropic roles, we next investigated whether SMC6 KO could rescue bortezomib effects on RC. Intriguingly, CRISPR SMC6 editing nearly completely rescued RC formation in bortezomib-treated cells (Figure 5G-I, S6A-B), suggesting that degradation of SMC6 is critical for EBV RC. Likewise, SMC6 KO significantly rescued RC formation in EBV+ Akata BNRF1 KO cells triggered for lytic reactivation by immunoglobulin crosslinking (Figure 5J-L, S6C-D) and also restored late gene gp350 expression (Figure S6E-F). Titers produced by BNRF1/SMC6 double KO were similar to those produced by Akata cells expressing paired control sgRNA against host and viral genome sites and stimulated by immunoglobulin cross-linking (Figure S6G).

To test the extent to which BNRF1 subversion of ATRX/DAXX might also be important for lytic replication, we used CRISPR to create BNRF1/ATRX double KO cells. In contrast to BNRF1/SMC6 double KO, BNRF1/ATRX double KO could not rescue plasma membrane gp350 expression, which is dependent on lytic EBV DNA replication in RC. Furthermore, ATRX KO also failed to rescue the production of infectious virion production in BNRF1/ATRX double KO Akata

cells (Fig. S6E-F). Therefore, our data suggests that SMC5/6 degradation, rather than targeting of ATRX/DAXX complexes, is the biologically key BNRF1 target that supports EBV lytic replication. (Figure S6G-H).

The SMC5/6 cohesin complex has multiple activities, including SUMO ligase, DNA entrapment and compaction (Yu et al., 2021). We therefore used CRISPR to investigate whether SMC5/6 components in addition to SMC6 were essential for restriction of RC. KO of the SUMO ligase subunit NSE2 partially restored RC formation in bortezomib-treated cells, suggesting that SUMOylation of a host or viral RC component is involved (Figure S7A-C). KO of the SMC5 subunit, which forms long filamentous structures with SMC6 (Figure 1B), rescued RC formation in bortezomib-treated cells to a similar extent as NSE2 KO. Similar results were obtained with KO of the non-SMC element (NSE) subunit NSE3, which forms a subcomplex together with NSE1 and NSE4 that binds to double stranded DNA (Figure S7A-C). These effects were also BNRF1 dependent, as KO of either SMC5 or NSE2 could at least partially rescue RC formation in BNRF1 edited Akata B-cells (Figure S7D-G). Collectively, these results suggest that EBV relies on BNRF1 to prevent entrapment as well as a SUMOylation event that counteracts RC.

SMC5/6 associates with R-loops in EBV replication compartments

A key question has remained how the SMC5/6 cohesin complex recognizes viral DNA. *In vitro*, SMC5/6 preferentially binds non-B form DNA and supercoiled substrates (Gutierrez-Escribano et al., 2020; Serrano et al., 2020). These can include R-loops, which are stable RNA: DNA hybrid triple stranded structures (Allison and Wang, 2019; Wang et al., 2018). We noted that conditional inactivation of the NSE4 subunit in budding yeast causes increased levels of R-loops (Chang et al., 2019), and that R-loops have key roles at γ-herpesvirus origins of lytic replication (o*riLyt*) in DNA replication, by allowing initial DNA strand separation and core replication protein loading (Rennekamp and Lieberman, 2011). We therefore hypothesized that BNRF1 is necessary to prevent SMC5/6 recognition of EBV lytic genomic R-loops.

To gain insights into the molecular mechanism by which the SMC5/6 complex inhibits the EBV lytic cycle, we stained cells with monoclonal antibody S9.6, which recognizes R-loops and double stranded RNA (dsRNA). In uninduced P3HR-1 cells, SMC6 highly co-localized with S9.6 signal in a peripheral nuclear distribution, presumably co-localizing with structures of host cell origin. By contrast, lytic induction redistributed S9.6 signal to nuclear foci. Conditionally over-expressed

SMC6, which we reasoned was expressed at a high enough level to overcome targeting by BNRF1, also redistributed to co-localizing nuclear puncta in reactivated cells (Figure 6A-B).

To then more specifically analyze S9.6 signal specific to R-loops, we treated cells with RNaseH, an endonuclease that digests DNA/RNA hybrid structures present at R-loops. RNase H strongly diminished the overall S9.6 signal, suggesting that it largely recognized R-loops in cells triggered for lytic replication (Figure 6C). RNase H also changed the subnuclear distribution of SMC6, suggesting that SMC6 substantially homes to RNA/DNA hybrids in lytic cells in the absence of RNase H. We next immunostained cells with the anti-dsRNA monoclonal antibody rJ2, in the absence or presence of RNase H pre-treatment. By contrast with that of S9.6, rJ2 dsRNA signal was not substantially affected by RNase H (Figure 6D-E). Moreover, SMC6 and S9.6 signals overlapped with nuclear DAPI, rather than with cytoplasmic F-actin staining, whereas rJ2 signals were predominantly perinuclear and cytoplasmic (Figure 6F-H). A large proportion of HA-SMC6 induced by 9 hours of doxycycline treatment co-immunoprecipitated with S9.6 (Cristini et al., 2018) in P3HR-1 concurrently induced for lytic reactivation (Figure 6I). Of note, whole cell HA-SMC6 abundances were low due to the short period of doxycycline induction and also due to its destabilization by EBV lytic reactivation, resulting in weak signals in lanes 2-5. Importantly, R-loop destruction by the addition of RNase H prevented SMC6 pulldown by S9.6. As a positive control, addition of benzonase, which degrades all forms of nucleic acid, also perturbed SMC6 co-immunoprecipitation with S9.6. Similarly, blockade of EBV lytic genome synthesis by addition of phosphonoacetic acid (PAA) prevented SMC6 co-immunoprecipitation (Figure 6I).

To directly test whether SMC6 associates with EBV lytic genomic R-loops, we performed chromatin immunoprecipitation (ChIP) for HA-epitope tagged SMC6 versus GFP control, followed by quantitative PCR for EBV *oriLyt*^{R}, which was previously found to contain an R-loop structure in reactivated cells (Rennekamp and Lieberman, 2011). ChIP-qPCR identified that SMC6 associated with *oriLyt*^{R} in cells induced for lytic replication, and this association was perturbed by addition of RNase H (Figure 6J). Interestingly, DNA conformation change, chromosome segregation and telomere organization were amongst the most enriched pathways identified by gene ontology analysis of differentially expressed host genes in control versus BNRF1 KO P3HR-1 cells induced for lytic replication (Figure 7A-B). Given well defined SMC6 roles in chromosome segregation, genome stability, alternative lengthening of the telomere and the ability of telomeres to form R-loop structures (Graf et al., 2017), we speculate that these mRNA changes directly arise from compensatory responses to BNRF1-mediated SMC6 depletion. These results support a

model where in the absence of BNRF1, SMC6 complexes recognize and occupy R-loops formed in the late lytic EBV cycle (Fig. 7C).

DISCUSSION

To periodically reactivate in immunocompetent hosts, EBV circumvents multiple layers of host defense, including intrinsic immune responses that sense and respond to foreign viral DNA. How EBV RC evade nuclear intrinsic immune pathways has remained an important question. In contrast to lipid-enclosed viral RC used by +sense RNA viruses that shield viral nucleic acids, EBV and other herpesviruses utilize nuclear membrane-less RC that are accessible to intrinsic immune responses. Our results position BNRF1 and the SMC5/6 cohesin complex as central players in the EBV host/pathogen interface (Figure 7C) and suggest that all herpesviruses may need to counteract SMC5/6 to support RC formation and lytic virus replication.

RC are seeded by single ~170 kb EBV genomes, which synthesize thousands of EBV genome copies. Our results suggest that BNRF1 circumvents SMC5/6 cohesin complexes from recognizing and suppressing lytic EBV genomes that seed and/or drive RC expansion. A similar phenomenon was also recently reported in adenovirus infected cells, in which the viral E4 early protein targets SMC6 for degradation. In the absence of E4, SMC6 associates with replicating adenoviral dsDNA genomes and impaired viral lytic DNA replication (Dybas et al., 2021). At early timepoints of lytic reactivation, EBV DNA templates are limiting for genome amplification and RC expansion (Nagaraju et al., 2019), and pharmacological blockade of lytic DNA replication collapses RC (Li et al., 2018). Thus, in the absence of BNRF1, SMC5/6 may suppress RC expansion by blocking lytic genome synthesis. This effect may also contribute to the increased numbers of empty capsids observed in BNRF1 KO cells, together with perturbed late gene expression. We speculate that BNRF1 has similarly important roles in supporting lytic replication in epithelial cells as well as in the establishment of B-cell latency, given profound SMC6 depletion in each of these settings. Indeed, in the absence of BNRF1, EBV latency gene expression is highly attenuated in newly infected B-cells (Feederle et al., 2006; Tsai et al., 2011), which may result not only from repressive effects of histone 3.3 by ATRX/DAXX, but also from SMC5/6 loading.

Use of a tegument protein, which is packaged in the virion and therefore primed to disarm the SMC5/6 complex without need for *de novo* EBV transcription or translation, provides EBV with a stealth approach. Likewise, BNRF1 expression during lytic replication again depletes SMC5/6 at

a time when it would otherwise recognize and counteract lytic genomes. This strategy provides a defined window during which EBV disrupts the SMC5/6 complex, typically in growth-arrested newly infected or lytic cells, perhaps limiting deleterious effects to host cells. Yet, EBV lytic replication is increasingly linked with cancer (Munz, 2019; Shannon-Lowe and Rickinson, 2019). For instance, elevated antibody titers against EBV lytic antigens are predictive of nasopharyngeal carcinoma (Chien et al., 2001). Similarly, the M81 EBV strain isolated from a nasopharyngeal carcinoma patient exhibits elevated levels of lytic replication (Tsai et al., 2013). Lytic reactivation contributes to transformed B-cell outgrowth *in vivo* in humanized mice models (Hong et al., 2005). Since SMC5/6 has key roles in host chromosome biology and DNA damage responses, our results provide a mechanism for the observation that BNRF1 can induce centrosome amplification and chromosomal instability in newly infected B-cells (Shumilov et al., 2017).

BNRF1 subversion of SMC5/6 may provide a mechanism by which EBV is associated with cancers, including by "hit-and-run" abortive infection. Such BNRF1 effects may connect to the clinical observation that infectious mononucleosis increases the risk of both EBV+ Hodgkin lymphoma and EBV-non-Hodgkin lymphoma over the first year post-infection (Ekstrom-Smedby, 2006; Hjalgrim et al., 2003). Atypical chromosomal structures and nuclear morphology are often noted in tissues of patients with active EBV infection, including in acute infectious mononucleosis (Watt et al., 1977). Although BNRF1 also disrupts ATRX-DAXX complexes (Tsai et al., 2011), this observation does not explain chromosomal instability observed during EBV infection and lytic replication, as DAXX only transiently colocalizes with centromeres (Morozov et al., 2012). By contrast, BNRF1 overexpression results in centrosome over-duplication (Shumilov et al., 2017).

In the absence of viral evasion, the SMC5/6 complex can restrict expression of dsDNA viral genomes, including those of herpes simplex virus, human papillomavirus, hepatitis B-virus and unintegrated HIV cDNA (Decorsiere et al., 2016; Dupont et al., 2021; Gibson and Androphy, 2020; Murphy et al., 2016; Xu et al., 2018). Yet, how SMC5/6 recognizes viral DNA has remained a key question, as specific sequences or structures that recruit SMC5/6 to viral genomes have not been identified. Recent *in vitro* studies suggest that yeast and human SMC5/6 cohesin complexes preferentially bind to non-B-form DNA, including highly supercoiled, catenated and plectoneme structures (Gutierrez-Escribano et al., 2020; Serrano et al., 2020). We present data that in cells undergoing lytic replication in the absence of BNRF1, SMC5/6 highly associated with signal from monoclonal antibody S9.6, which recognizes R-loops and dsRNA.

R-loops are triple stranded RNA: DNA hybrid structures that have been linked to genome instability (Bayona-Feliu et al., 2021; Chen et al., 2017), whereas SMC5/6 have major roles as

guardians of chromosome stability. Our experiments with RNase H pretreatment support R-loops, rather than dsRNA, as the major SMC5/6 cohesin complex target in lytic B-cells. EBV origins of lytic replication contain G-rich regions, which are pre-requisites for RNA: DNA hybrid structures, and R-loops form at these regions in lytic EBV genomes (Rennekamp and Lieberman, 2011). Computational analysis performed on 6000 viruses suggests that >70% of dsDNA viruses encode R-loop forming sequences, including all viruses in the *Herpesvirales* order (Wongsurawat et al., 2020). These observations suggest a potentially central mechanism for SMC5/6 recruitment to herpesvirus genomes in the absence of viral evasion. By contrast, SMC5/6 is recruited to unintegrated HIV proviral genomes by the adaptor protein SLF2, perhaps because such cDNA does not have non-B-form DNA regions such as R-loops (Dupont et al., 2021).

How SMC5/6 disrupts expression of EBV late genes remains an objective for future studies. Our data support a model where upon recognition of EBV R-loop and perhaps other non-B-form DNA structures formed in lytic replication, SMC5/6 complexes are loaded onto circular EBV genomes templates for lytic replication in the absence of BNRF1. This may impair the production of linear lytic genomes, resulting in diminished late gene expression and decreased viral loads. It remains plausible that SMC5/6 are also loaded onto linear genomes produced by the EBV DNA polymerase to impair their packaging into viral capsids, perhaps by DNA compaction.

Unexpectedly, BNRF1 juxtaposes calpain and SMC5/6 complexes. Calpains are Ca^{2+}-dependent cysteine proteases that can mark substrates for proteasomal degradation by the Arg/N-end rule pathway (Piatkov et al., 2014; Shemorry et al., 2013; Varshavsky, 2011). We suspect that calpain SMC6 cleavage exposes an N-terminal degron signal that leads to its Cul7-mediated ubiquitin-proteasome degradation. It is noteworthy that BNRF1 targets SMC5/6 and ATRX/DAXX by distinct mechanisms. Interestingly, the murine gamma-herpesvirus homolog tegument protein ORF75c induces PML degradation to support viral gene expression (Ling et al., 2008). It is plausible that different BNRF1 pools carry out these two important antiviral functions. Alternatively, use of distinct BNRF1 surfaces for SMC6 versus DAXX association may allow preferential calpain recruitment to the SMC5/6 interface.

We note that bacterial artificial chromosome EBV genomic BNRF1 KO did not apparently reduce EBV viral load in a HEK-293 cell system (Feederle et al., 2006). 293 cells lack multiple DNA sensors such as cGAS/STING, and we observed low levels of SMC6 by immunoblot of 293 whole cell lysates, perhaps obviating the need for BNRF1 in this system. We observed SMC6 loss in AGS gastric carcinoma cells induced for lytic replication (Figure 1D) and suspect that BNRF1 has similarly important roles in support of epithelial cell lytic replication.

How can the late gene BNRF1 be important for expression of other EBV late genes as well as have a role in DNA replication, which is initiated in the early lytic period? First, we note that while CAGE-seq studies suggest BNRF1 is expressed with late gene kinetics in HEK-293 cells with EBV BAC genomes (Djavadian et al., 2018), independent studies have also identified its expression in lymphoblastoid cell lines with the latency III program (Abbott et al., 2013; Adhikary et al., 2020). Low basal BNRF1 levels may have important roles even within early phases of B-cell lytic cycles. We suspect that an initial burst of late gene synthesis likely produces the empty capsids observed by electron microscopy. Second, while late gene transcription precedes significant increases in EBV DNA copy number, ongoing DNA replication is necessary for sustained late gene expression (Li et al., 2018). Therefore, BNRF1 may be required to maintain ongoing late gene expression.

In conclusion, the EBV major tegument protein BNRF1 is critical for defense of membrane-less nuclear replication compartments against the activity of SMC5/6 cohesins. There is increasing interest in lytic induction approaches that leverage the presence of EBV genomes to sensitize tumors to the antiviral agents or to targeted CD8+ T-cell killing (Feng et al., 2004). However, induction of virion production carries the risk of delivering BNRF1 to neighboring cells. Therefore, where the goal is to sensitize tumors to adoptively transferred anti-EBV T-cells against the highly immunogenic EBV immediate early BZLF1, it may be prudent to consider use acyclovir or ganciclovir to block EBV late gene expression. This approach could minimize DNA damage to neighboring cells caused by delivery of BNRF1 and SMC5/6 depletion.

Limitations of the study.

A key limitation of this study is that to our knowledge, monoclonal 9.6 is the only antibody that visualizes R-loops, but it also recognizes additional structures, in particular dsRNA. We attempted to establish R-loop specificity of our 9.6 results by inclusion of experiments with RNase H, an endonuclease that cleaves RNA at RNA/DNA hybrids and is therefore specific for R-loop structures. Nonetheless, additional studies should be performed with R-loop specific reagents as they become available. Similarly, knowledge remains incomplete about early events that enable rapid EBV lytic DNA amplification perhaps prior to rolling circle amplification. It remains plausible that additional non-B-form DNA structures formed by EBV lytic replication are sensed by SMC5/6, which could include plectoneme structures. Secondly, precise mechanism by which SMC5/6 restricts EBV RC and late gene expression in the absence of BNRF1 remain to be established. Additional studies are needed to ascertain whether SMC5/6 topological DNA entrapment is sufficient, or whether EBV DNA is compacted by SMC5/6 complexes. Similarly, precise

SUMOylation roles, which our CRISPR KO studies suggest to also be important for SMC5/6 antiviral activity, remain to be established. Thirdly, additional studies are required to establish whether BNRF1 targeting of SMC5/6 is necessary for establishment of latency, licensing of EBV oncoprotein induction and/or the initial phases of growth transformation in newly infected primary human B-cells. The recent development of primary human B-cell CRISPR editing techniques should facilitate these studies.

Acknowledgements

We thank Maria Ericsson in the Harvard Medical School Electron Microscopy core for assistance with electron microscopy images. We thank Sankar Swaminathan for the AGSiZ cell line and Jaap Middeldorp for antibodies. This work was supported by NIH RO1s AI137337, AI 164709 and CA228700 and a Burroughs Wellcome Career Award in Medical Sciences to BEG, and by a Lymphoma Research Foundation award to R.G. M.P.W. is supported by a Wellcome Trust Senior Clinical Research Fellowship (108070/Z/15/Z). This research was funded in whole, or in part, by the Wellcome Trust [Wellcome Senior Clinical Research Fellowship 108070/Z/15/Z to MPW]. For the purpose of open access, the author has applied a CC BY public copyright licence to any Author Accepted Manuscript version arising from this submission. RNA-seq data was deposited in NIH GEO Omnibus GSE182349 and will be released upon publication.

Author Contributions.

S.P.T.Y performed and analyzed the experiments. S.P.T.Y. performed the RNA-seq experiments, which were analyzed by R.G. S.P.T.Y. and C.Z performed the proteomic experiments, which were analyzed by S.P.T.Y, C.Z, M.P.W and B.E.G. Bioinformatic analysis was performed by S.P.T.Y, R.G., C.Z. M.P.W. and B.E.G supervised the study. S.P.T.Y and B.E.G wrote the manuscript.

Declaration of Interests

The authors declare no competing interests. BEG receives support from an Abbvie-Harvard grant for research unrelated to these studies.

Figure Legends

Figure 1. The SMC5/6 cohesin complex is depleted by incoming EBV and lytic replication.

(A) Waterfall plot illustrating log2 fold change in protein abundances of P3HR-1 host proteins that significantly change ($p<0.05$) at 24 hours post-lytic reactivation.

(B) Schematic illustration of the SMC5/6 complex.

(C) Temporal proteomic plots of SMC5/6 complex abundances in mock induced (red) or ZHT/RHT P3HR-1 cells induced for lytic replication by 4HT that express the late gene gp350 (green) or that did not become gp350+ (orange). Error bars ±SEM (n=3 replicates).

(D) Immunoblot analysis of whole cell lysates (WCL) from EBV+ AGS cells with conditional BZLF1 allele induced for lytic replication by doxycycline (2 µg/ml) for 48hr.

(E) Plot of -log2 fold change in protein abundances of host proteins that were significantly different in proteomic analysis of primary human B-cells infected by B95.8 EBV at 48 hours of infection versus in resting B-cells.

(F) Temporal proteomic plots of SMC5/6 complex abundances at the indicated days post primary human B-cell EBV infection. Data show the mean ±SEM, n=4.

(G) Immunoblot of SMC6 vs DDX46 load control values in primary (top) or Daudi B-cells at 0 versus 3 days post infection (DPI). Blots in D and G are representative of n=2 replicates. See also Figure S1.

See also Figure S1.

Figure 2. EBV tegument protein BNRF1 targets SMC5/6 for proteasomal degradation in a calpain-dependent manner.

(A) Volcano plot analysis of changes in proteomic abundances in primary human B-cells at Day 2 post-infection vs uninfected.

(B) Relative BNRF1 protein abundances at the indicated days post primary B-cell EBV infection.
(C) Immunoblot analysis of WCL from P3HR-1 cells mock induced or doxycycline (dox, 5 ug/ml) induced for EBV lytic gene cDNA expression for 24 hours.

(D) Immunoblot analysis of WCL from Cas9+ P3HR-1 ZHT/RHT cells expressing the indicated sgRNA and mock induced or induced for lytic reactivation by 4-HT (400nM) and sodium butyrate (NaB, 500 µM) for 24 hours.

(E) Immunoblot analysis of P3HR-1 ZHT/RHT WCL from cells mock induced or doxycycline induced for BNRF1 cDNA expression, in the presence of bortezomib (5nM) or MLN4924 (10 µM), as indicated, for 24hrs.

(F) BNRF1-selective protein interactors identified by affinity purification, HA peptide elution and mass spectrometry analysis of doxycycline-induced HA-BNRF1 in P3HR-1 ZHT/RHT cells induced for lytic replication by 4HT/NaB, and cross-compared with HA-tagged tegument protein controls BPLF1 or BOLF1.

(G) Immunoblot analysis of 1% input and anti-HA immunopurified GFP or SMC6 complexes from P3HR-1 untreated or treated with doxycycline (5µg/ml) and bortezomib (5nM) for 6hrs, as indicated. Representative of two independent experiments.

(H) Immunoblot analysis of WCL from P3HR-1 cells with doxycycline-induced HA-tagged BNRF1 and treated with bortezomib, MLN4924, or calpeptin for 24 hrs, as indicated.

(I) Immunoblot analysis of WCL from P3HR-1 ZHT/RHT cells expressing the indicated sgRNAs and induced for lytic replication, as indicated. Blots are representative of n=2 independent replicates unless otherwise indicated. See Also Figure S2.

See also Figure S2.

Figure 3. BNRF1 associates with SMC6.

(A) Immunoblot analysis of 1% input and anti-HA immunopurified complexes from P3HR-1 untreated or induced for GFP vs BNRF1 with doxycycline (5µg/ml) for 6 hours and treated with bortezomib (5nM) for 6hrs. Representative of two independent experiments.

(B) Immunofluorescence analysis of HA-tagged SMC6 and doxycycline-induced V5-tagged BNRF1 versus nuclear DAPI signals in EBV+ Akata cells treated with bortezomib (5 nM) and MLN4924 (10 µM) for 12hrs. Scale bar: 2 µm. Representative of n=3 experiments.

(C) Schematic of BNRF1 wildtype (WT) and deletion mutant constructs used.

(D) Immunoblot analysis of WCL from P3HR-1 cells untreated or induced for BNRF1 cDNA expression by doxycycline (5 µg/ml) for 24hrs. Representative of n=2 replicates.

(E) Immunofluorescence analysis of HA-tagged BNRF1 expression doxycycline induced in P3HR-1 cells (5 µg/ml) for 24h vs DAPI. Zoomed images of cells boxed in white are shown in the top two rows. Representative of n=3 experiments. See Also Figure S3.

See also Figure S3.

Figure 4. BNRF1 supports late lytic cycle progression, viral DNA replication and infectious virion production.

(A) Heatmap of normalized EBV gene expression levels from RNA-seq analysis of P3HR-1 ZHT/RHT cells with control or BNRF1 sgRNA, mock induced or induced into lytic cycle with 4-HT/NaB for 24hrs, from n=2 replicates.

(B) Flow cytometry analysis of plasma membrane (PM) gp350 expression in P3HR-1 expressing control BXLF1 or BNRF1 sgRNAs, mock induced or induced for lytic reactivation for 24 hours with 4HT/NaB.

(C) Mean error bars ±SEM PM gp350 in P3HR-1 cells obtained as in B from n=5 replicates.

(D) qRT-PCR of EBV intracellular genome copy number from P3HR-1 cells with BXLF1 or BNRF1 sgRNA induced by 4HT/NaB for 24 hours. Mean ±SEM values from n=3 replicates are shown.

(E) Transmission electron microscopy (TEM) of P3HR-1 cells with control or BNRF1 sgRNAs induced into lytic cycle with 4-HT/NaB for 24hrs. Scale bar: 500nm.

(F) Percentage of empty capsids observed from TEM analysis of P3HR-1 cells with control vs. BNRF1 sgRNA, as in E. Data are from n=20 randomly chosen nuclear fields.

(G) Mean ±SEM from n=3 replicates of green Raji assay analysis of infectious EBV titers from EBV+ Akata with BXLF1 or BNRF1 sgRNA induced by IgG crosslinking or 48 hours from n=3 replicates. ****$p < 0.0001$. **$p < 0.01$. See Also Figure S4.

See also Figure S4.

Figure 5. BNRF1 is critical for viral replication compartment formation.

(A) Immunofluorescence analysis of replication compartment (RC), as judged by EdC-labelled DNA and by staining for BMRF1 in P3HR-1 ZHT/RHT cells that expressed the indicated sgRNAs induced into by 4HT/NaB for 24hrs. Zoom images of cells in white boxes shown at bottom.

(B) 3D reconstruction of EdC and BMRF1 signals as in A, using the Image J Interactive 3D Surface Plot package. Scalebar indicates fluorescence intensity.

(C) Mean ±SEM percentages of nuclei with RC from N=3 replicates, as in A, using data from 20 randomly selected panels off 200 nuclei, using ImageJ.

(D) RC Immunofluorescence analysis as in (A), using P3HR-1 ZHT/RHT cells that expressed the indicated sgRNAs and rescue BNRF1 cDNA.

(E) 3D reconstruction of EdC and BMRF1 signals as in D, using the Image J Interactive 3D Surface Plot package. Scalebar indicates fluorescence intensity.

(F) Mean ±SEM percentages of nuclei with RC from N=3 replicates, as in D, using data from 20 randomly selected panels off 200 nuclei, using ImageJ.

(G) RC Immunofluorescence analysis as in (A), using P3HR-1 ZHT/RHT cells that expressed no sgRNA, control or SMC6 sgRNA, or BNRF1 sgRNA and rescue BNRF1 cDNA and were treated with bortezomib, as indicated.

(H) 3D reconstruction of EdC and BMRF1 signals as in G, using the Image J Interactive 3D Surface Plot package. Scalebar indicates fluorescence intensity.

(I) Mean ±SEM percentages of nuclei with RC from N=3 replicates, as in G, using data from 20 randomly selected panels off 200 nuclei, using ImageJ.

(J) RC Immunofluorescence analysis as in (A), using P3HR-1 ZHT/RHT cells that the indicated sgRNAs.

(K) 3D reconstruction of EdC and BMRF1 signals as in J, using the Image J Interactive 3D Surface Plot package. Scalebar indicates fluorescence intensity.

(L) Mean ±SEM percentages of nuclei with RC from N=3 replicates, as in D, using data from 20 randomly selected panels off 200 nuclei, using ImageJ.

See Also Figure S5-7.

Figure 6. SMC6 associates with EBV genomic R-loop regions in the absence of BNRF1.

(A) Confocal immunofluorescence analysis of P3HR-1 ZHT/RHT cells stained with S9.6, anti-SMC6-HA, or DAPI. S9.6 recognizes R-loops and double stranded RNA (dsRNA). Cells were not induced for exogenous SMC6-HA (- Dox) or for lytic reactivation (-4-HT/NaB). Representative of three independent experiments.

(B) Confocal analysis of P3HR-1 ZHT/RHT cells treated with doxycycline (5 µg/ml) to induce exogenous SMC6 expression and with 4HT/NaB for 9hrs to induce EBV lytic reactivation, as indicated. Cells were then stained with S9.6, anti-HA-SMC6 or DAPI. Representative of three independent experiments.

(C) Confocal analysis of cells as in (B) that were pre-incubated with RNaseH (5U/µg DNA) prior to staining with S9.6, anti-HA or DAPI. Representative of three independent experiments.

(D) Confocal analysis of cells as in (B) and stained with anti-dsRNA antibody rJ2 or DAPI. Representative of three independent experiments.

(E) Confocal analysis of cells as in (B) that were pre-incubated with RNase H (5U/µg DNA) prior to staining with anti-dsRNA antibody rJ2 or DAPI. Representative of three independent experiments.

(F) Confocal analysis of cells as in (B) and stained with S9.6, anti-F-actin or DAPI. Representative of three independent experiments.

(G) Confocal analysis of cells as in (B), stained with anti-dsRNA antibody rJ2, anti-HA-SMC6, anti-F-actin or DAPI, as indicated. Representative of three independent experiments.

(H) Confocal analysis of cells as in (B) that were pre-incubated with RNase H (5U/µg DNA) prior to staining with anti-dsRNA antibody rJ2, anti-HA-SMC6, anti-F-actin or DAPI. Representative of three independent experiments.

(I) Immunoblot analysis of 1% input and S9.6-immunopurified complexes from P3HR-1 ZHT/RHT cells induced for exogenous HA-SMC6 and treated with 4HT/NaB and phosphonacetic acid (PAA, 200µg/ml) for 9 hours, as indicated. Samples were treated with RNase H (5.5U/µg DNA) or benzonase (5U/µg DNA) prior to IP, as indicated.

(J) Mean ±SEM values from n=3 replicates of ChIP-qPCR analysis of SMC6 occupancy at the EBV genomic *oriLyt*^{R} region. Anti-HA ChIP was performed on chromatin from EBV+ Akata cells

with stable SMC6-HA or GFP-HA expression following 48 hours of αIgG crosslinking, followed by qPCR using *oriLyt*^{R} region specific primers. *p<0.05.

Figure 7. BNRF1 KO effects on lytic cycle host and viral gene expression.

(A) RNAseq volcano plot analysis of host mRNA abundances in P3HR-1 ZHT/RHT cells that expressed control versus BNRF1 sgRNAs and that were induced by 4HT/NaB for 24h, as in Fig. 4A. Circles represent individual host mRNA values. Transcripts encoding proteins involved in DNA conformation change, chromosome segregation and mitosis are highlighted.

(B) Gene ontology (GO) biological process enrichment analysis of host mRNAs differentially expressed in P3HR-1 ZHT/RHT cells with control versus BNRF1 sgRNAs and induced by 4HT/NaB for 24h, as in Fig. 4A.

(C) Schematic model of BNRF1 evasion of SMC5/6 complexes in lytic replication. BNRF1 produced upon late lytic cycle progression associates with calpain and Cul7 to target the SMC5/6 cohesin complex for ubiquitin-proteasome pathway degradation. In the absence of BNRF1, the SMC5/6 complex associates with EBV genomic R-loops including at the origin of lytic replication and perhaps additional non-B-form DNA structures formed in lytic replication to prevent sustained late gene expression, replication compartment formation, EBV lytic genome encapsidation and infectious virion assembly.

Star Methods

RESOURCE AVAILABILITY

LEAD CONTACT

Further information and requests for resources and reagents should be directed to and will be fulfilled by the Lead Contact, Benjamin E. Gewurz (bgewurz@bwh.harvard.edu).

MATERIALS AVAILABILITY

All reagents will be made available on request after completion of a Materials Transfer Agreement.

DATA AND CODE AVAILABILITY

- All RNA-seq datasets have been deposited to the NIH GEO omnibus (GSE182349) and are publicly available as of the date of publication. All raw data have been deposited at Mendeley and are publicly available as of the date of publication (DOI: 10.17632/5v545cw8t7.1). Microcopy data reported in this paper will be shared by the lead contact upon request. Figures were drawn with commercially available GraphPad, Biorender and Microsoft Powerpoint.
- This paper does not report original code.
- Any additional information required to reanalyze the data reported in this paper is available from the lead contact upon request.

EXPERIMENTAL MODEL AND SUBJECT DETAILS

Cell Lines

HEK293T were cultured in DMEM supplemented with 10% FBS and 1% Pen/Strep. AGSiZ were cultured in F-12-Glutomax supplemented with 10% FBS, 1% Pen/Strep, 0.5 µg/ml puromycin and 0.5 mg/ml G418. P3HR-1-ZHT/RHT-Cas9+, EBV+ Akata-Cas9+, BJAB-Cas9+ and Daudi-Cas9+ cells were cultured in RPMI-1640 supplemented with 10% v/v FBS and 1% Pen/Strep. Cas9+ cells were maintained in 5 µg/ml blasticidin. P3HR-1-Z/R-HT were also maintained with 25 µg/ml G418 and 25 µg/ml hygromycin. All cells were incubated at 37ºC with 5% CO_2 and were routinely confirmed to be mycoplasma-negative. Cell lines were authenticated by STIR profiling. cDNA used in this study were cloned into the pLIX-402 or pLX-TRC313 vector. pLIX-402 uses a Tet ON TRE promoter to drive expression of the gene of interest with a C-terminal HA Tag. pLX_TRC313 uses a EF1α promoter to drive expression of the gene of interest with a C-terminal V5 tag. Stable cell lines were generated by lentiviral transduction and antibiotic selection with puromycin (pLIX-402) or hygromycin (pLX_TRC313). Cell lines were then maintained with 0.5 µg/ml puromycin or 25µg/ml hygromycin.

METHOD DETAILS

Molecular cloning

Unless otherwise specified, all cloning experiments were performed by Gateway recombination. Briefly, 150ng of the destination vector and donor vector containing the gene of interest were co-

incubated with 1X LR Clonase Enzyme Mix (Invitrogen #11789-020) overnight at room temperature. The reaction mixture was then transformed into 50µl of Stbl3 bacteria, spread on LB plates with ampicillin.

CRIPSR analysis

CRISPR/Cas9 editing was performed as described (Guo et al., 2020). Briefly, sgRNAs were cloned into pLentiGuide-puro (Addgene plasmid #52963 (Sanjana et al., 2014)) or pLenti-spBsmBI-sgRNA-Hygro (Addgene plasmid #62205 (Pham et al., 2016)) by restriction-ligation, and sequenced verified. Lentiviral transduction in 293T cells were performed as described previously (Ersing et al., 2017). In brief, 293T cells were co-transfected with 500ng lentiviral plasmid, 400ng psPAX2 (Plasmid #12260) and 150ng VSV-G plasmids for packaging. Lentivirus produced were filtered with 0.45µm filter and transduced into P3HR-1-Z/R-HT-Cas9+ and Akata-EBV-Cas9+ cells. Transduced cells were selected for 1 week with puromycin or 2 weeks with hygromycin. CRISPR KOs were verified by western blot analysis or T7EI endonuclease assay (only when antibody is unavailable). sgRNA against the above-mentioned genes are listed in the supplementary table.

cDNA Rescue

BNRF1 rescue cDNA in entry vector, with silent PAM mutations at BNRF1 sg1, is described in the following table. BNRF1 sg#1 targeting sequence are highlighted; while PAM sequence and mutations sites are underlined and indicated in red, respectively. Mutations were performed with Q5 Site-Directed Mutagenesis Kit (NEB) and sequence verified. Rescue BNRF1 cDNA in entry vector was cloned into pLX-TRC313 vector (a gift from John Doench) by Gateway recombination. BNRF1 rescue cDNA was confirmed by western blot analysis using anti-V5 tag antibody. Oligo sequences for cDNA rescue used in this study are listed in the supplementary table. .

BNRF1 deletion mutants

A collection of 300aa BNRF1 cDNA deletion in entry vector were generated with PrimeSTAR GXL Premix (Takara Bio) according to manufacturer's instructions, using primers listed in the following. Deletions were sequenced verified and were cloned into pLX402 vector by Gateway recombination. Expression of BNRF1-mutant were induced by 5 µg/ml doxycycline and verified by western blot analysis using anti-HA antibody. Oligonucleotide sequences used for performing BNRF1 mutagenesis are listed in the supplementary table. .

Primary human B-cell isolation and infection

Platelet-depleted venous blood was obtained from the Brigham and Women's Hospital Blood Bank, following our Institutional Review Board-approved protocol for discarded and de-identified samples. RosetteSep and EasySep negative isolation kits (STEMCELL Technologies) were used

sequentially to isolate CD19+ B-cells with modifications made to the manufacturer's protocols as described previously (Wang et al., 2019b). For proteomic analysis, primary B-cells were infected by B95.8 EBV, as described (Wang et al., 2019a). For validation studies of BNRF1 depletion upon B-cell infection, EBV B95.8 virus was produced from 293-EBV-BAC producer cells by co-transfecting plasmids expressing BZLF1 and BALF4 for 24 hrs, followed by treatment with 12-O-tetradecanoylphorbol-13-acetate (TPA, 20ng/ml) and NaB (2mM) for an addition of 72 hrs. Supernatant were collected and filtered through a 0.45 µm filter. Virus were concentrated 200-fold by ultracentrifugation. EBV titer was determined experimentally by transformation assay. EBV was added to 1M purified B cells at an MOI of 0.8 for 72hrs, incubated at 37ºC with 5% CO_2. Cells were harvested and 10% were subjected to flow cytometry analysis for infection efficiency, while the remaining were used for western blot analysis.

Immunoblot analysis

Whole cell lysates were separated by SDS-PAGE electrophoresis, transferred onto nitrocellulose membrane, blocked with 5% milk in TBST buffer for 1 hr and incubated with the corresponding primary antibodies at 4ºC overnight. Blots were washed 3 times in TBST solution and were incubated with secondary antibodies for 1 hr at room temperature. Blots were then washed 3 times in TBST solution and were developed by incubating with ECL chemiluminescence. Images were captured by Licor Fc platform. All antibodies used in this study are listed in the Key Resources table.

Flow cytometry analysis

Cells were washed once with cold PBS supplemented with 2% v/v fetal bovine serum (FBS). Cells were then incubated with PE-conjugated anti-CD23 (1:250) or Cy5-conjugaged anti-gp350 antibody (1:1000) in 2% FBS v/v, PBS for 30 mins at 4ºC. Cell were pelleted, washed twice, resuspended in 2% FBS v/v, PBS into flow cytometry-compatible tubes and processed immediately. Flow cytometric data was acquired with a BD FACSCalibur instrument and analysis was performed with FlowJo V10.

Immunofluorescence analysis

Cells dried on glass slides were fixed with 4% paraformaldehyde/PBS solution for 10 min, permeabilized with 0.5% Triton X-100/PBS for 5 min and blocked with 1% BSA/PBS for 1 hr at room temperature. For experiments involving RNase H treatment, cells were blocked with 1% BSA/PBS supplemented with 500U/µg DNA RNase H (NEB) for 1 hr at 37ºC. Subsequently, cells

were incubated with a cocktail of primary antibodies against BMRF1 (0.4 µg/ml), HA (1:1000) or V5 (1:1000) in blocking solution for 1 hr at 37ºC. Cells were then washed twice with PBS and incubated with a cocktail of secondary antibodies at 1:500 in PBS for 1 hr at 37ºC in the dark. Finally, cells were washed twice with PBS and were stained/mounted overnight with ProLong™ Gold Antifade Mountant with DAPI. Image acquisition and analysis was performed with Zeiss LSM 800 instrument and with Zeiss Zen Lite (Blue) software, respectively. 3D reconstruction of Figure 4A using Arivis Vision4D from ZEISS ZEN lite (blue edition). Image J was used to score the % of nuclei with RC in P3HR-1 cells, using the ImageJ "Particle Analysis" plugin. For 5-Ethynyl-2'-deoxycytidine (EdC) labelling of newly synthesized DNA**,** EDC (5 µM) was added together with lytic induction stimuli. Click chemistry was performed to conjugate biotin to the EdC, as described previously (Cabral et al., 2018). In brief, subsequent to secondary antibodies staining, cells were washed twice with PBS. Biotin conjugation to EdC was performed by incubating the cells with PBS supplemented with 200µM CuSo4, 1mM sodium ascorbate and 25µg/ml biotin azide for 2 hrs at 37ºC in dark. Cells were then washed twice with PBS and incubated with streptavidin-conjugated antibodies (1:1000) in PBS for 30 mins at 37ºC in dark. Finally, cells were washed twice with PBS and were stained/mounted overnight with ProLong™ Gold Antifade Mountant with DAPI.

Green Raji and Daudi assay

Green Raji and Daudi assays were performed as previously described (Altmann and Hammerschmidt, 2005; Pich et al., 2019). In brief, EBV lytic replication was induced by anti-human IgG (15 µg/ml) and supernatant were collected and filtered through 0.8 µm filters at 72 hrs post induction. 0.1 million/ml Raji or Daudi cells were infected at MOI 0.9. At 24 hrs post infection, culture media were exchanged to fresh RPMI supplemented with 10% FBS and cells were treated with 20 ng/ml tetradecanoyl phorbol acetate (TPA) and 3mM NaB for another 48 hrs. Cells were collected and the percentage of GFP+ cells were determined by flow cytometry.

Quantification of EBV copy number

Intracellular EBV genome copy # were quantified by qPCR analysis. For intracellular viral DNA extraction, total DNA from $1x10^6$ cells were extracted by the Blood & Cell culture DNA mini kit (Qiagen). Extracted DNA were diluted to 10 ng/µl and were subjected to qPCR targeting the BALF5 gene. Serial dilutions of pHAGE-BALF5 plasmid at 25 ng/µl were used to generate the standard curve. Viral DNA copy number was calculated by substituting sample Cq values into the

regression equation dictated by the standard curve. qPCR primer sequences used for DNA copy number quantification are listed in the supplementary table.

T7 endonuclease I (T7EI) assay

T7EI assay was performed using EnGen Mutation Detection Kit (NEB) following manufacturer's protocol. Briefly, genomic DNA was first extracted from cells expressing sgControl or sgRNA that targets BXLF1. Cas9-targeted regions were then PCR amplified. The amplified products were separated by gel electrophoresis, extracted, and purified using QIAquick® Gel Extraction Kit (Qiagen). Equal amount of PCR products from control and BXLF1 KO samples were mixed and were added with 1 µl NEB2 buffer. The mixture was then subjected to 95°C for 10 mins and then cooled down to 4°C at a cooling rate of 0.1°C/ s in a Thermocyler. 0.25U T7EI was added to the product and was incubated for 1 hr at 37ºC. The final reaction product was then separated by gel electrophoresis. Images were captured using Licor Fc platform.

Co-immunoprecipitation analysis

Expression of SMC6, BNRF1 or the collection of BNRF1 mutants were induced by the addition of 5 ug/ml doxycycline. Bortezomib was added to prevent the degradation of SMC6 during BNRF1 expression or EBV lytic induction. 150M cells were harvested and was lysed in cold lysis buffer (1% v/v NP40, 150mM Tris, 300mM NaCl in dH2O) supplemented with 1X cOmplete™ EDTA-free protease inhibitor cocktail (Sigma), 1mM Na3VO4 and 1mM NaF for 1 hr at 4ºC with rotation. Lysed cells were pelleted, and lysates were incubated with anti-HA tag magnetic beads (Pierce, Thermo) at 4ºC overnight. Beads were washed with lysis buffer for four times and were eluted using 1X SDS loading buffer incubated for 10 mins at 95ºC. Proteins were separated by SDS-PAGE gel and transferred to nitrocellulose membranes. Subsequent procedures were similar to that mentioned in "Western blot analysis"

Poly-Ubiquitinylation co-immunoprecipitation analysis

Cells were induced into lytic replication by 2mM 4HT/500µM NaB and were either untreated or treated with 5nM Bortezomib or 50µM Calpeptin for 16 hrs. 150M cells were harvested and was lysed in cold lysis buffer (1% v/v NP40, 150mM Tris, 300mM NaCl in dH2O) supplemented with 1X cOmplete™ EDTA-free protease inhibitor cocktail (Sigma), 1mM Na3VO4, 1mM NaF, 1mM

PMSF, 4mM 1, 10 o-phenanthroline, 2mM sodium pyrophosphate and 1mM EDTA for 1 hr at 4ºC with rotation. Lysed cells were pelleted and precleared with protein A/G magnetic beads (Pierce, Thermo). Precleared lysate was then incubated with anti-poly-ubiquitin antibody (Cell signaling, P4D1) for 1 hr at 4ºC with rotation. Protein A/G magnetic beads were then added to the immunocomplex and were incubated at 4ºC overnight. Beads were washed with lysis buffer for four times and were eluted using 1X SDS loading buffer incubated for 10 mins at 95ºC. Proteins were separated by SDS-PAGE gel and transferred to nitrocellulose membranes. Subsequent procedures were similar to that mentioned in "Western blot analysis".

R-loop co-immunoprecipitation analysis

SMC6 expression was induced by the addition of 5 µg/ml doxycycline to P3HR-1-Z/R-HT-Cas9+ cells (established with pLX402-SMC6). EBV lytic cycle were induced with procedures mentioned in "reactivation of EBV lytic cycle". 200 µg/ml PAA was added where indicated. R-loop-IP was performed as described previously (Cristini et al., 2018). Briefly, $50x10^6$ of these cells were harvested. They were non-crosslinked and were lysed in lysis buffer (85 mM KCl, 5 mM PIPES (pH 8.0), and 0.5% v/v NP-40) for 10 mins at 4ºC with rotation. Pelleted nuclei were resuspended in resuspension buffer (10 mM Tris-HCl pH 7.5, 200 mM NaCl, 2.5 mM MgCl2, 0.2% w/v sodium deoxycholate [NaDOC], 0.1% v/v SDS, 0.05% w/v sodium lauroyl sarcosinate [Na sarkosyl] and 0.5% v/v Triton X-100). The extracts were then sonicated (10s on, 10s off, 10 cycles) by an ultra-sonication processor (Diagenode, USA). The sonicated extracts were then diluted 1:2 in RSB+T buffer (10 mM Tris-HCl pH 7.5, 200 mM NaCl, 2.5 mM MgCl2 and 0.5% v/v Triton X-100) and were subjected to IP with the S9.6 antibody (Millipore) together with protein A/G magnetic beads (Pierce, Thermo) that were washed three times with RSB+T buffer and pre-blocked with 0.5% BSA-PBS for 2 hrs at 4ºC. Where indicated, 5.5U RNase H per mg of DNA or 1U/µl benzonase were added to the samples before IP for 1 hr at 37ºC with rotation. Beads were washed four times with RSB+T buffer, twice with RSB buffer and were eluted in 1X SDS loading buffer for 10 mins at 95ºC. Eluted proteins were separated by SDS-PAGE with procedures similar to "Western blot analysis".

Chromatin immunoprecipitation (ChIP)-qPCR

Fifty million P3HR-1-Z/-R-HT-Cas9+ (established with either pLX402-SMC6, pLX402-GFP or BNRF1-KO/pLX402-SMC6) were fixed with 1% PFA (at final concentration) for 10 mins at room temperature. 0.4M (working concentration) of glycine was then added to the fixed cells and incubated for an addition of 5 mins at room temperature. Cells were lysed with lysis buffer ()

supplemented with cOmplete™ EDTA-free protease inhibitor cocktail (Sigma) for 1 hr at 4ºC. They were then fragmented by an ultra-sonication processor (Diagenode, USA). Soluble chromatin was diluted and incubated with 40 µl anti-HA magnetic beads (Pierce, Thermo) overnight at 4ºC. Beads were extensively washed and eluted with elution buffer (100mM NaHCO3 and 1% SDS in dH2O). Reverse cross-linking was performed by protease K treatment (40 U/ml) at 65ºC overnight. DNA was then purified by QIAquick PCR purification kit (Qiagen). ChIP assay DNA was qPCR quantified and normalized to the percent of input DNA. Primer sequences used for ChIP-qPCR performed in this study are listed in the supplementary table .

RNA sequencing (RNA-seq) experiments

Total RNA was isolated using RNeasy mini kit (Qiagen) following manufacturer's instructions. In-column DNA digestion was included to remove residual genomics DNA contamination. To construct indexed libraries, 1 µg of total RNA was used for polyA mRNA-selection using NEBNext Poly(A) mRNA Magnetic Isolation Module (NEB), followed by library construction using NEBNext Ultra RNA Library Prep Kit for Illumina (NEB). Each experimental treatment was performed in biological triplicate. Libraries were multi-indexed, pooled and sequenced on an Illumina NextSeq 500 sequencer using single-end 75 bp reads (Illumina). All raw sequencing reads were first evaluated using FastQC (http://www.bioinformatics.babraham.ac.uk) and confirmed with no significant quality issues. For RNA-seq data analysis, paired-end reads were mapped to human (GENCODE v28) and EBV (Akata) transcriptome and quantified using Salmon v0.8.2 (Patro et al., 2017) under quasi-mapping and GC bias correction mode. Read count table of human and EBV genes was then normalized across compared cell lines/conditions and differentially expressed genes were evaluated using DESeq2 v1.18.1 (Love et al., 2014) under default settings. Pathway analysis was performed by using WebGestalt (WEB-based Gene SeT AnaLysis Toolkit) functional enrichment analysis web tool under default setting (Liao et al., 2019).

Transmission electron microscopy

A pellet of cells was fixed for at least 2 hrs at RT in fixative (2.5% Glutaraldehyde 1.25% Paraformaldehyde and 0.03% picric acid in 0.1 M sodium cacodylate buffer (pH 7.4)), washed in 0.1M cacodylate buffer and post-fixed with 1% Osmiumtetroxide (OsO4)/1.5% Potassiumferrocyanide (KFeCN6) for 1 hr, washed 2x in water, 1x Maleate buffer (MB) 1x and

incubated in 1% uranyl acetate in MB for 1 hr followed by 2 washes in water and subsequent dehydration in grades of alcohol (10 mins each; 50%, 70%, 90%, 2x10 mins 100%). The samples were then put in propyleneoxide for 1 hr and infiltrated overnight in a 1:1 mixture of propyleneoxide and TAAB (TAAB Laboratories Equipment Ltd, https://taab.co.uk). The following day the samples were embedded in TAAB Epon and polymerized at 60°C for 48 hrs. Ultrathin sections (about 60 nm) were cut on a Reichert Ultracut-S microtome, picked up on to copper grids stained with lead citrate and examined in a JEOL 1200EX Transmission electron microscope or a TecnaiG^{2} Spirit BioTWIN and images were recorded with an AMT 2k CCD camera.

Sample preparation for LC/MS analysis

Whole cell lysates were prepared from 400 million P3HR-1 ZHT/RHT cells (per replicate) that were induced into the lytic cycle by 4HT (400 nM)/NaB (500 µM) for 24hrs and that were also conditionally induced to express HA-tagged BPLF1, BOLF1 or BNRF1 by doxycycline (5 µg/ml) for 15hrs. Samples were prepared as previously mentioned (Nobre et al., 2019). In brief, 400M cells per replicate cells expressing either BNRF1-HA, BOLF1-HA, BPLF1-HA or BLRF2-HA were induced into lytic cycle and were harvested and lysed in (50 mM Tris-HCl pH 7.5, 300 mM NaCl, 0.5% v/v NP40, 1 mM DTT and Roche protease inhibitor cocktail). Samples were tumbled for 15 mins at 4°C and subjected to centrifugation at 16000xg for 15 mins at 4°C. Lysates were then filtered through a 0.7 µm filter and incubated for 3 hrs with immobilized mouse monoclonal anti-HA agarose resin (Sigma). Duplicates samples were combined and washed seven times with lysis buffer, followed by seven PBS washes. After that, proteins bound to the anti-HA resin were eluted twice by adding 200 µl of 250 µg/ml HA peptide in PBS at 37°C for 30 mins with agitation. Finally, proteins were precipitated with 20% Trichloroacetic acid (TCA), washed once with 10% TCA, washed three times with cold acetone and dried to completion using a centrifugal evaporator. Samples were then resuspended in digestion buffer (50 mM Tris-HCl pH 8.5, 10% acetonitrile (AcN), 1 mM DTT, 10 µg/ml Trypsin (Promega) and incubated overnight at 37°C with agitation. The reaction was quenched with 50% formic acid (FA), subjected to C18 solid-phase extraction, and vacuum-centrifuged to complete dryness. Samples were reconstituted in 4% AcN/5% FA and divided into technical duplicates prior to LC-MS/MS on an Orbitrap Lumos.

LC-MS Analysis

Peptides for each sample were analyzed in technical duplicate, with the run order reversed from one batch of replicate analyses to the next to ensure that any carry-over was different in each case. Two washes were used between each sample to further minimize carry-over. Mass

spectrometry data were acquired using an Orbitrap Fusion Lumos. An Ultimate 3000 RSLC nano UHPLC equipped with a 300 µm ID x 5 mm Acclaim PepMap µ-Precolumn (Thermo Fisher Scientific) and a 75 µm ID x 75 cm 2 µm particle Acclaim PepMap RSLC analytical column was used. Loading solvent was 0.1% v/v FA, and the analytical solvents were (A) 0.1% v/v FA and (B) 80% v/v AcN + 0.1% v/v FA. All separations were carried out at 55°C. Samples were loaded at 5 µl/min for 5 min in loading solvent before beginning the analytical gradient. The following gradient was used: 3–7% B over 3 min then 7–37% B over 54 min followed by a 4 min wash in 95% B and equilibration in 3% B for 15 min. The following settings were used: MS1, 350–1500 Thompsons (Th), 120,000 resolution, 2 × 105 automatic gain control (AGC) target, 50 ms maximum injection time. MS2, quadrupole isolation at an isolation width of m/z 0.7, higher-energy collisional dissociation (HCD) fragmentation (normalized collision energy (NCE) 34) with fragment ions scanning in the ion trap from m/z 120, 1 × 104 AGC target, 250 ms maximum injection time, with ions accumulated for all parallelizable times. The method excluded undetermined and very high charge states (≥25+). Dynamic exclusion was set to + /- 10 ppm for 25 s. MS2 fragmentation was trigged on precursors 5 × 103 counts and above. Two 45 min washes were included between every affinity purification-mass spectrometry (AP-MS) analysis, to minimize carry-over between samples. 1 µl transport solution (0.1% v/v trifluoroacetic acid) was injected, over the following gradient: 3–40% B over 29 min followed by a 3 min wash at 95% B and equilibration at 3% B for 10 min.

CompPASS identification of high confidence protein interactors.

To identify interactors for each bait, replicate pairs were combined to attain a summary of proteins identified in both runs. Data reported for each protein in every IP in the dataset include: (a) the number of peptide spectrum matches (PSMs) averaged between technical replicates; (b) an entropy score, which compares the number of PSM between replicates to eliminate proteins that are not detected consistently; (c) a z-score, calculated in comparison to the average and standard deviation of PSMs observed across all IPs; and (d) an NWD score, which reflects (i) how frequently this protein was detected and (ii) whether it was detected reproducibly. NWD scores were calculated as described in (Behrends et al., 2010) using the fraction of runs in which a protein was observed, the observed number of PSMs, the average and standard deviation of PSMs observed for that protein across all IPs, and the number of replicates (1 or 2) containing the protein of interest. Protein interactors identified were filtered with false discovery rate (FDR) <0.02; average peptide spectrum match ≥1.5; entropy score ≥0.75 and top 2% WD/z-score.

977 ## QUANTIFICATION AND STATISTICAL ANALYSIS

978 Unless otherwise indicated, all bargraphs and linegraphs represent the arithmetic mean of three
979 independent experiments (n = 3), with error bars denoting SEM. Significance between the control
980 and experimental groups, or indicated pairs of groups, was assessed using the unpaired Student's
981 t test in the GraphPad Prism 7 software. P values correlate with symbols as follows, unless
982 otherwise indicated: ns = not significant, p > 0.05; *p % 0.05; **p % 0.01; ***p % 0.001; ****p %
983 0.0001. Principal Component Analysis (PCA) of RNA-seq datasets were determined and
984 visualized using R 3.3.2. Pathway analysis was performed and visualized by using WebGestalt
985 functional enrichment analysis web tool.

986 ## KEY RESOURCES TABLE

REAGENT or RESOURCE	SOURCE	IDENTIFIER
Antibodies		
Anti-ATRX rabbit monoclonal antibody (D1N2E)	Cell Signaling Technology	#14820; RRID: AB_2798630
Anti-BNRF1 rabbit monoclonal antibody	A gift from Paul Lieberman	N/A
Anti-BMRF1 mouse monoclonal antibody	A gift from Jaap M Middeldorp	N/A
Anti-EBV ZEBRA mouse monoclonal antibody (BZ1)	Santa Cruz Biotechnology	sc-53904; RRID: AB_783257
Anti-CAPN1 mouse monoclonal antibody	Proteintech Group	67732-1-Ig
Anti-CAPNS1 rabbit polyclonal antibody	Proteintech Group	25057-1-AP; RRID: AB_2879876
Anti-human CD23 Antibody (PE conjugate)	Biolegend	338507; RRID: AB_1279179
Anti-DAXX rabbit monoclonal antibody (25C12)	Cell Signaling Technology	#4533; RRID: AB_2088778
Anti-DDX46 rabbit polyclonal antibody	Proteintech Group	16927-1-AP; RRID: AB_2090927
Anti-GAPDH XP® rabbit monoclonal (D16H11)	Cell Signaling Technology	AB_10622025
Anti-gp350 mouse monoclonal antibody	A gift from Jaap M Middeldorp	N/A
Anti-HA.11 tag mouse monoclonal antibody (16B12)	Biolegend	901513; RRID: AB_2820200
Anti-NSMCE2 rabbit polyclonal antibody	Proteintech Group	13627-1-AP; RRID: AB_10637854
Anti-NDNL2(NSMCE3) rabbit polyclonal antibody	Proteintech Group	27488-1-AP; RRID: AB_2880885
Anti-PARP rabbit monoclonal antibody (46D11)	Cell Signaling Technology	#9532; RRID: AB_659884
Anti-DNA-RNA hybrid antibody (S9.6)	Millipore	MABE1095; RRID: AB_2861387
Anti-SMC5 rabbit polyclonal antibody	Proteintech Group	14178-1-AP; RRID: AB_2192775

Anti-SMC6L1 rabbit monoclonal antibody	Boster Biological Technology	A01554-1
Anti-V5-Tag rabbit monoclonal antibody (D3H8Q)	Cell Signaling Technology	#13202; RRID: AB_2687461
Anti-Mouse IgG HRP-coupled secondary antibody	Cell Signaling Technology	7076
Anti-Rabbit IgG HRP-coupled secondary antibody	Cell Signaling Technology	7074
Anti-dsRNA mouse monoclonal antibody (clone rJ2)	Millipore	MABE1134
Anti-Ubiquitin mouse monoclonal antibody (P4D1)	Cell Signaling Technology	3936
Goat anti-Rabbit IgG (H+L) Cross-Adsorbed Secondary Antibody, Alexa Fluor 568	Thermo Fisher Scientific	A-11011; RRID: AB_141416
Goat anti-Mouse IgG (H+L) Cross-Adsorbed Secondary Antibody, Alexa Fluor 488	Thermo Fisher Scientific	A-11001; RRID: AB_143160
Anti-streptavidin, Alexa Fluor 647 conjugate	Thermo Fisher Scientific	S32357
Anti-Human IgG rabbit polyclonal antibody (Gamma-Chains)	Agilent	A042402; RRID: AB_578517
Bacterial and virus strains		
EBV BAC WT	Bo Zhao	N/A
Chemicals, peptides, and recombinant proteins		
Pierce™ Protein A/G Magnetic Beads	Thermo Fisher Scientific	88803
Pierce™ Anti-HA Magnetic Beads	Thermo Fisher Scientific	88837
T4 DNA ligase	New England Biolabs	M0202L
Proteinase K	New England Biolabs	P8107S
Doxycycline hyclate	Sigma-Aldrich	D9891-1G
(Z)-4-Hydroxytamoxifen	Sigma-Aldrich	H7904-25MG
Sodium butyrate, >98%, Alfa Aesar™	Thermo Fisher Scientific	AAA1107922
NAE Inhibitor, MLN4924	Sigma-Aldrich	5.05477
Bortezomib (PS-341)	APExBIO	A2614
InSolution™ Leupeptin, Hemisulfate, Microbial	Millipore	509281
E-64 protease inhibitor	Millipore	324890-5MG
Calpeptin ≥98% (HPLC)	Millipore	C8999
5-Ethynyl-2'-deoxycytidine, (EdC)	Sigma-Aldrich	T511307-5MG
Biotin Picolyl Azide	Click Chemistry Tools	1167-25
Cupric Sulfate Pentahydrate	Thermo Fisher Scientific	C489-500
Sodium ascorbate	Sigma-Aldrich	A4034-500G
RNase H	New England Biolabs	M0297L
Phosphonoacetic acid (PAA)	Sigma-Aldrich	284270-10G
Benzonase® Nuclease	Sigma-Aldrich	E1014-5KU
Exonuclease T	New England Biolabs	M0265S
T7 Endonuclease I	New England Biolabs	M0302S
DNase I	Roche	10104159001
Formaldehyde solution	Sigma-Aldrich	F8775
cOmplete™, Mini, EDTA-free Protease Inhibitor Cocktail	Roche	11697498001

Puromycin Dihydrochloride	Thermo Fisher Scientific	A1113803
Hygromycin B	Millipore	400052
G418 Sulfate Solution (50 mg/mL)	GeminiBio	400113
Blasticidin	InvivoGen	ant-bl-5
TransIT®-LT1 Transfection Reagent	Mirus Bio	MIR 2306
NP40	Sigma-Aldrich	74385-1L
Sequencing Grade Modified Trypsin (Mass Spec Grade) (lyophilized)	Promega	V5111-5x20µg
HA Synthetic Peptide	Thermo Fisher Scientific	26184-5mg
Monoclonal Anti-HA−Agarose antibody produced in mouse	Sigma-Aldrich	A2095-1ML
Critical commercial assays		
RNeasy Mini Kit	Qiagen	74104
Cy5® Conjugation Kit (Fast)	Abcam	Ab188288
QiAquick PCR Purification Kit	Qiagen	28106
Blood & Cell Culture DNA Maxi Kit	Qiagen	13362
QIAprep Spin Miniprep Kit	Qiagen	27106
DNeasy Blood& Tissue Kit	Qiagen	69504
QIAquick Gel Extraction Kit	Qiagen	28704
RNase-Free DNase Set	Qiagen	79254
iScript Reverse Transcription Supermix for RT-qPCR	BIO-RAD	1708841
Power SYBR Green PCR Master Mix	Applied Biosystems	4367659
Gateway™ LR Clonase™ II Enzyme Mix	Invitrogen	11789-020
NEBNext® Poly(A) mRNA Magnetic Isolation Module	New England Biolabs	E7490S
NEBNext® Ultra™ II Directional RNA Library Prep with Sample Purification Beads	New England Biolabs	E7765S
NEBNext® Multiplex Oligos for Illumina® (Index Primers Set 2)	New England Biolabs	E7500S
NEBNext® Multiplex Oligos for Illumina® (Index Primers Set 1)	New England Biolabs	E7335S
EasySep™ Human T Cell Isolation Kit	Stemcell Technologies	17954
RosetteSep™ Human Monocyte Enrichment Cocktail	Stemcell Technologies	15064
Deposited data		
RNAseq	This paper	GSE182349
Mendeley dataset	This paper	DOI: 10.17632/5v545cw8t7.1
Experimental models: Cell lines		
EBV+ Burkitt lymphoma P3HR-1 ZHT	A gift from Eric Johannsen	N/A
EBV+ Burkitt lymphoma AKATA-Cas9	Guo et al., 2020	N/A
EBV+ Burkitt lymphoma Daudi-Cas9	Ma et al., 2017	N/A
HEK293T	ATCC	CRL-3216
EBV+ Gastric carcinoma AGSiZ	A gift from Sankar Swaminathan	N/A
EBV+ Burkitt lymphoma Raji	ATCC	ATCC® CCL-86™
EBV- Burkitt lymphoma BJAB-Cas9	A gift from Bo Zhao	N/A
Oligonucleotides		

sgRNAs were listed in Supplementary Table	This paper	N/A
Primers for BNRF1 cDNA rescue were listed in Supplementary Table	This paper	N/A
Mutagenesis primers were listed in Supplementary Table	This paper	N/A
qPCR primers for EBV copy number quantification were listed in Supplementary Table	This paper	N/A
ChIP-qPCR primers were listed in Supplementary Table	This paper	N/A
Recombinant DNA		
pLentiGuide-Puro	A gift from Feng Zhang (Sanjana et al., 2014)	Addgene_52963
pLenti SpBsmBI sgRNA Hygro	A gift from Rene Maehr (Pham et al., 2016)	Addgene_62205
pLX-TRC313	Broad Institute	N/A
pLX-402	Broad Institute	N/A
pENTR-BNRF1	Eric Johannsen	N/A
pENTR-BRLF1	Eric Johannsen	N/A
pENTR-BLLF3	Eric Johannsen	N/A
pENTR-BGLF4	Eric Johannsen	N/A
pENTR-GFP	Eric Johannsen	N/A
pENTR-BOLF1	Eric Johannsen	N/A
pENTR-BPLF1	Eric Johannsen	N/A
pENTR-SMC6	DNASU	HsCD00080486
pLX-402-BNRF1	This paper	N/A
pLX-TRC313-BNRF1	This paper	N/A
pLX-402-BRLF1	This paper	N/A
pLX-402-BLLF3	This paper	N/A
pLX-402-BGLF4	This paper	N/A
pLX-402-GFP	This paper	N/A
pLX-402-BOLF1	This paper	N/A
pLX-402-BPLF1	This paper	N/A
pLX-402-SMC6	This paper	N/A
Software and algorithms		
Salmon v0.8.2	Patro et al., 2017	https://combine-lab.github.io/salmon/
DESeq2 v1.18.1	Love et al., 2014	https://bioconductor.org/packages/release/bioc/html/DESeq2.html
WebGestalt (WEB-based Gene SeT AnaLysis Toolkit)	Liao et al., 2019	http://www.webgestalt.org/
GraphPad Prism 7	GraphPad Software	https://www.graphpad.com/scientific-software/prism/
Flowjo X	Flowjo LLC.	https://www.flowjo.com/
Biorender	Biorender	https://biorender.com/
ImageJ	ImageJ	https://imagej.nih.gov/ij/

ImageJ- Particle Analyzer	ImageJ	https://imagej.net/imaging/particle-analysis
ImageJ- Interactive 3D Surface Plot	Kai Uwe Barthel	https://imagej.nih.gov/ij/plugins/surface-plot-3d.html
Zeiss Zen Lite (Blue)	Zeiss	https://www.zeiss.com/microscopy/int/products/microscope-software/zen-lite.html
Arivis Vision4D	Arivis	https://imaging.arivis.com/en/imaging-science/arivis-vision4d
Other		
Standard Fetal Bovine Serum, Qualified, USDA-Approved Regions	Thermo Fisher Scientific	10437028
RPMI 1640 Medium	Life Technologies	11875085
DMEM, high glucose, pyruvate	Life Technologies	11995081
Ham's F-12 Nutrient Mix, GlutaMAX™ Supplement	Thermo Fisher Scientific	31765035

REFERENCES:

Abbott, R.J., Quinn, L.L., Leese, A.M., Scholes, H.M., Pachnio, A., and Rickinson, A.B. (2013). CD8+ T cell responses to lytic EBV infection: late antigen specificities as subdominant components of the total response. J Immunol *191*, 5398-5409.

Adhikary, D., Damaschke, J., Mautner, J., and Behrends, U. (2020). The Epstein-Barr Virus Major Tegument Protein BNRF1 Is a Common Target of Cytotoxic CD4(+) T Cells. J Virol *94*.

Allison, D.F., and Wang, G.G. (2019). R-loops: formation, function, and relevance to cell stress. Cell Stress *3*, 38-46.

Altmann, M., and Hammerschmidt, W. (2005). Epstein-Barr virus provides a new paradigm: a requirement for the immediate inhibition of apoptosis. PLoS Biol *3*, e404.

Bayona-Feliu, A., Barroso, S., Munoz, S., and Aguilera, A. (2021). The SWI/SNF chromatin remodeling complex helps resolve R-loop-mediated transcription-replication conflicts. Nat Genet *53*, 1050-1063.

Behrends, C., Sowa, M.E., Gygi, S.P., and Harper, J.W. (2010). Network organization of the human autophagy system. Nature *466*, 68-76.

Bentley, P., Tan, M.J.A., McBride, A.A., White, E.A., and Howley, P.M. (2018). The SMC5/6 Complex Interacts with the Papillomavirus E2 Protein and Influences Maintenance of Viral Episomal DNA. J Virol *92*.

Buschle, A., and Hammerschmidt, W. (2020). Epigenetic lifestyle of Epstein-Barr virus. Semin Immunopathol *42*, 131-142.

Cabral, J.M., Oh, H.S., and Knipe, D.M. (2018). ATRX promotes maintenance of herpes simplex virus heterochromatin during chromatin stress. Elife *7*.

Chakravorty, A., Sugden, B., and Johannsen, E.C. (2019). An Epigenetic Journey: Epstein-Barr Virus Transcribes Chromatinized and Subsequently Unchromatinized Templates during Its Lytic Cycle. J Virol *93*.

1011 Chang, E.Y., Tsai, S., Aristizabal, M.J., Wells, J.P., Coulombe, Y., Busatto, F.F., Chan, Y.A., Kumar, A., Dan
1012 Zhu, Y., Wang, A.Y.*, et al.* (2019). MRE11-RAD50-NBS1 promotes Fanconi Anemia R-loop suppression at
1013 transcription-replication conflicts. Nat Commun *10*, 4265.
1014 Chen, L., Chen, J.Y., Zhang, X., Gu, Y., Xiao, R., Shao, C., Tang, P., Qian, H., Luo, D., Li, H.*, et al.* (2017). R-
1015 ChIP Using Inactive RNase H Reveals Dynamic Coupling of R-loops with Transcriptional Pausing at Gene
1016 Promoters. Mol Cell *68*, 745-757 e745.
1017 Chien, Y.C., Chen, J.Y., Liu, M.Y., Yang, H.I., Hsu, M.M., Chen, C.J., and Yang, C.S. (2001). Serologic markers
1018 of Epstein-Barr virus infection and nasopharyngeal carcinoma in Taiwanese men. N Engl J Med *345*, 1877-
1019 1882.
1020 Cristini, A., Groh, M., Kristiansen, M.S., and Gromak, N. (2018). RNA/DNA Hybrid Interactome Identifies
1021 DXH9 as a Molecular Player in Transcriptional Termination and R-Loop-Associated DNA Damage. Cell Rep
1022 *23*, 1891-1905.
1023 Daikoku, T., Kudoh, A., Fujita, M., Sugaya, Y., Isomura, H., Shirata, N., and Tsurumi, T. (2005). Architecture
1024 of replication compartments formed during Epstein-Barr virus lytic replication. J Virol *79*, 3409-3418.
1025 Decorsiere, A., Mueller, H., van Breugel, P.C., Abdul, F., Gerossier, L., Beran, R.K., Livingston, C.M., Niu, C.,
1026 Fletcher, S.P., Hantz, O.*, et al.* (2016). Hepatitis B virus X protein identifies the Smc5/6 complex as a host
1027 restriction factor. Nature *531*, 386-389.
1028 Djavadian, R., Chiu, Y.F., and Johannsen, E. (2016). An Epstein-Barr Virus-Encoded Protein Complex
1029 Requires an Origin of Lytic Replication In Cis to Mediate Late Gene Transcription. PLoS Pathog *12*,
1030 e1005718.
1031 Djavadian, R., Hayes, M., and Johannsen, E. (2018). CAGE-seq analysis of Epstein-Barr virus lytic gene
1032 transcription: 3 kinetic classes from 2 mechanisms. PLoS Pathog *14*, e1007114.
1033 Dupont, L., Bloor, S., Williamson, J.C., Cuesta, S.M., Shah, R., Teixeira-Silva, A., Naamati, A., Greenwood,
1034 E.J.D., Sarafianos, S.G., Matheson, N.J.*, et al.* (2021). The SMC5/6 complex compacts and silences
1035 unintegrated HIV-1 DNA and is antagonized by Vpr. Cell Host Microbe *29*, 792-805 e796.
1036 Dybas, J.M., Lum, K.K., Kulej, K., Reyes, E.D., Lauman, R., Charman, M., Purman, C.E., Steinbock, R.T.,
1037 Grams, N., Price, A.M.*, et al.* (2021). Adenovirus Remodeling of the Host Proteome and Host Factors
1038 Associated with Viral Genomes. mSystems, e0046821.
1039 Ekstrom-Smedby, K. (2006). Epidemiology and etiology of non-Hodgkin lymphoma--a review. Acta Oncol
1040 *45*, 258-271.
1041 Ersing, I., Nobre, L., Wang, L.W., Soday, L., Ma, Y., Paulo, J.A., Narita, Y., Ashbaugh, C.W., Jiang, C., Grayson,
1042 N.E.*, et al.* (2017). A Temporal Proteomic Map of Epstein-Barr Virus Lytic Replication in B Cells. Cell Rep
1043 *19*, 1479-1493.
1044 Farrell, P.J. (2019). Epstein-Barr Virus and Cancer. Annu Rev Pathol *14*, 29-53.
1045 Feederle, R., Neuhierl, B., Baldwin, G., Bannert, H., Hub, B., Mautner, J., Behrends, U., and Delecluse, H.J.
1046 (2006). Epstein-Barr virus BNRF1 protein allows efficient transfer from the endosomal compartment to
1047 the nucleus of primary B lymphocytes. J Virol *80*, 9435-9443.
1048 Feng, W.H., Hong, G., Delecluse, H.J., and Kenney, S.C. (2004). Lytic induction therapy for Epstein-Barr
1049 virus-positive B-cell lymphomas. J Virol *78*, 1893-1902.
1050 Gibson, R.T., and Androphy, E.J. (2020). The SMC5/6 Complex Represses the Replicative Program of High-
1051 Risk Human Papillomavirus Type 31. Pathogens *9*.
1052 Graf, M., Bonetti, D., Lockhart, A., Serhal, K., Kellner, V., Maicher, A., Jolivet, P., Teixeira, M.T., and Luke,
1053 B. (2017). Telomere Length Determines TERRA and R-Loop Regulation through the Cell Cycle. Cell *170*, 72-
1054 85 e14.
1055 Guo, R., Jiang, C., Zhang, Y., Govande, A., Trudeau, S.J., Chen, F., Fry, C.J., Puri, R., Wolinsky, E., Schineller,
1056 M.*, et al.* (2020). MYC Controls the Epstein-Barr Virus Lytic Switch. Mol Cell *78*, 653-669 e658.

1057 Gutierrez-Escribano, P., Hormeno, S., Madariaga-Marcos, J., Sole-Soler, R., O'Reilly, F.J., Morris, K., Aicart-
1058 Ramos, C., Aramayo, R., Montoya, A., Kramer, H.*, et al.* (2020). Purified Smc5/6 Complex Exhibits DNA
1059 Substrate Recognition and Compaction. Mol Cell *80*, 1039-1054 e1036.
1060 Hammerschmidt, W., and Sugden, B. (2013). Replication of Epstein-Barr viral DNA. Cold Spring Harb
1061 Perspect Biol *5*, a013029.
1062 Hjalgrim, H., Askling, J., Rostgaard, K., Hamilton-Dutoit, S., Frisch, M., Zhang, J.S., Madsen, M., Rosdahl, N.,
1063 Konradsen, H.B., Storm, H.H.*, et al.* (2003). Characteristics of Hodgkin's lymphoma after infectious
1064 mononucleosis. N Engl J Med *349*, 1324-1332.
1065 Hong, G.K., Gulley, M.L., Feng, W.H., Delecluse, H.J., Holley-Guthrie, E., and Kenney, S.C. (2005). Epstein-
1066 Barr virus lytic infection contributes to lymphoproliferative disease in a SCID mouse model. J Virol *79*,
1067 13993-14003.
1068 Huang, H., Deng, Z., Vladimirova, O., Wiedmer, A., Lu, F., Lieberman, P.M., and Patel, D.J. (2016). Structural
1069 basis underlying viral hijacking of a histone chaperone complex. Nat Commun *7*, 12707.
1070 Huttlin, E.L., Ting, L., Bruckner, R.J., Gebreab, F., Gygi, M.P., Szpyt, J., Tam, S., Zarraga, G., Colby, G., Baltier,
1071 K.*, et al.* (2015). The BioPlex Network: A Systematic Exploration of the Human Interactome. Cell *162*, 425-
1072 440.
1073 Kenney, S.C., and Mertz, J.E. (2014). Regulation of the latent-lytic switch in Epstein-Barr virus. Semin
1074 Cancer Biol *26*, 60-68.
1075 Li, D., Fu, W., and Swaminathan, S. (2018). Continuous DNA replication is required for late gene
1076 transcription and maintenance of replication compartments in gammaherpesviruses. PLoS Pathog *14*,
1077 e1007070.
1078 Liao, Y., Wang, J., Jaehnig, E.J., Shi, Z., and Zhang, B. (2019). WebGestalt 2019: gene set analysis toolkit
1079 with revamped UIs and APIs. Nucleic Acids Res *47*, W199-W205.
1080 Lieberman, P.M. (2013). Keeping it quiet: chromatin control of gammaherpesvirus latency. Nat Rev
1081 Microbiol *11*, 863-875.
1082 Ling, P.D., Tan, J., Sewatanon, J., and Peng, R. (2008). Murine gammaherpesvirus 68 open reading frame
1083 75c tegument protein induces the degradation of PML and is essential for production of infectious virus.
1084 J Virol *82*, 8000-8012.
1085 Love, M.I., Huber, W., and Anders, S. (2014). Moderated estimation of fold change and dispersion for RNA-
1086 seq data with DESeq2. Genome Biol *15*, 550.
1087 Meng, Q., Hagemeier, S.R., Fingeroth, J.D., Gershburg, E., Pagano, J.S., and Kenney, S.C. (2010). The
1088 Epstein-Barr virus (EBV)-encoded protein kinase, EBV-PK, but not the thymidine kinase (EBV-TK), is
1089 required for ganciclovir and acyclovir inhibition of lytic viral production. J Virol *84*, 4534-4542.
1090 Miller, I.G., Jr., and El-Guindy, A. (2002). Regulation of Epstein-Barr virus lytic cycle activation in malignant
1091 and nonmalignant disease. J Natl Cancer Inst *94*, 1733-1735.
1092 Morozov, V.M., Gavrilova, E.V., Ogryzko, V.V., and Ishov, A.M. (2012). Dualistic function of Daxx at
1093 centromeric and pericentromeric heterochromatin in normal and stress conditions. Nucleus *3*, 276-285.
1094 Munz, C. (2019). Latency and lytic replication in Epstein-Barr virus-associated oncogenesis. Nat Rev
1095 Microbiol *17*, 691-700.
1096 Murphy, C.M., Xu, Y., Li, F., Nio, K., Reszka-Blanco, N., Li, X., Wu, Y., Yu, Y., Xiong, Y., and Su, L. (2016).
1097 Hepatitis B Virus X Protein Promotes Degradation of SMC5/6 to Enhance HBV Replication. Cell Rep *16*,
1098 2846-2854.
1099 Nagaraju, T., Sugden, A.U., and Sugden, B. (2019). Four-dimensional analyses show that replication
1100 compartments are clonal factories in which Epstein-Barr viral DNA amplification is coordinated. Proc Natl
1101 Acad Sci U S A *116*, 24630-24638.
1102 Nikitin, P.A., Yan, C.M., Forte, E., Bocedi, A., Tourigny, J.P., White, R.E., Allday, M.J., Patel, A., Dave, S.S.,
1103 Kim, W.*, et al.* (2010). An ATM/Chk2-mediated DNA damage-responsive signaling pathway suppresses
1104 Epstein-Barr virus transformation of primary human B cells. Cell Host Microbe *8*, 510-522.

1105 Niu, C., Livingston, C.M., Li, L., Beran, R.K., Daffis, S., Ramakrishnan, D., Burdette, D., Peiser, L., Salas, E.,
1106 Ramos, H.*, et al.* (2017). The Smc5/6 Complex Restricts HBV when Localized to ND10 without Inducing an
1107 Innate Immune Response and Is Counteracted by the HBV X Protein Shortly after Infection. PLoS One *12*,
1108 e0169648.
1109 Nobre, L.V., Nightingale, K., Ravenhill, B.J., Antrobus, R., Soday, L., Nichols, J., Davies, J.A., Seirafian, S.,
1110 Wang, E.C., Davison, A.J.*, et al.* (2019). Human cytomegalovirus interactome analysis identifies
1111 degradation hubs, domain associations and viral protein functions. Elife *8*.
1112 Ono, Y., and Sorimachi, H. (2012). Calpains: an elaborate proteolytic system. Biochim Biophys Acta *1824*,
1113 224-236.
1114 Parkin, D.M. (2006). The global health burden of infection-associated cancers in the year 2002. Int J Cancer
1115 *118*, 3030-3044.
1116 Patro, R., Duggal, G., Love, M.I., Irizarry, R.A., and Kingsford, C. (2017). Salmon provides fast and bias-
1117 aware quantification of transcript expression. Nat Methods *14*, 417-419.
1118 Pham, H., Kearns, N.A., and Maehr, R. (2016). Transcriptional Regulation with CRISPR/Cas9 Effectors in
1119 Mammalian Cells. Methods Mol Biol *1358*, 43-57.
1120 Piatkov, K.I., Oh, J.H., Liu, Y., and Varshavsky, A. (2014). Calpain-generated natural protein fragments as
1121 short-lived substrates of the N-end rule pathway. Proc Natl Acad Sci U S A *111*, E817-826.
1122 Pich, D., Mrozek-Gorska, P., Bouvet, M., Sugimoto, A., Akidil, E., Grundhoff, A., Hamperl, S., Ling, P.D., and
1123 Hammerschmidt, W. (2019). First Days in the Life of Naive Human B Lymphocytes Infected with Epstein-
1124 Barr Virus. mBio *10*.
1125 Qu, D., Wang, G., Wang, Z., Zhou, L., Chi, W., Cong, S., Ren, X., Liang, P., and Zhang, B. (2011). 5-Ethynyl-
1126 2'-deoxycytidine as a new agent for DNA labeling: detection of proliferating cells. Anal Biochem *417*, 112-
1127 121.
1128 Rennekamp, A.J., and Lieberman, P.M. (2011). Initiation of Epstein-Barr virus lytic replication requires
1129 transcription and the formation of a stable RNA-DNA hybrid molecule at OriLyt. J Virol *85*, 2837-2850.
1130 Rixon, F.J., and Schmid, M.F. (2014). Structural similarities in DNA packaging and delivery apparatuses in
1131 Herpesvirus and dsDNA bacteriophages. Curr Opin Virol *5*, 105-110.
1132 Sanjana, N.E., Shalem, O., and Zhang, F. (2014). Improved vectors and genome-wide libraries for CRISPR
1133 screening. Nat Methods *11*, 783-784.
1134 Serrano, D., Cordero, G., Kawamura, R., Sverzhinsky, A., Sarker, M., Roy, S., Malo, C., Pascal, J.M., Marko,
1135 J.F., and D'Amours, D. (2020). The Smc5/6 Core Complex Is a Structure-Specific DNA Binding and
1136 Compacting Machine. Mol Cell *80*, 1025-1038 e1025.
1137 Shannon-Lowe, C., and Rickinson, A. (2019). The Global Landscape of EBV-Associated Tumors. Front Oncol
1138 *9*, 713.
1139 Shannon-Lowe, C., Rickinson, A.B., and Bell, A.I. (2017). Epstein-Barr virus-associated lymphomas. Philos
1140 Trans R Soc Lond B Biol Sci *372*.
1141 Shemorry, A., Hwang, C.S., and Varshavsky, A. (2013). Control of protein quality and stoichiometries by N-
1142 terminal acetylation and the N-end rule pathway. Mol Cell *50*, 540-551.
1143 Shumilov, A., Tsai, M.H., Schlosser, Y.T., Kratz, A.S., Bernhardt, K., Fink, S., Mizani, T., Lin, X., Jauch, A.,
1144 Mautner, J.*, et al.* (2017). Epstein-Barr virus particles induce centrosome amplification and chromosomal
1145 instability. Nat Commun *8*, 14257.
1146 Speck, S.H., Chatila, T., and Flemington, E. (1997). Reactivation of Epstein-Barr virus: regulation and
1147 function of the BZLF1 gene. Trends Microbiol *5*, 399-405.
1148 Sugimoto, A., Sato, Y., Kanda, T., Murata, T., Narita, Y., Kawashima, D., Kimura, H., and Tsurumi, T. (2013).
1149 Different distributions of Epstein-Barr virus early and late gene transcripts within viral replication
1150 compartments. J Virol *87*, 6693-6699.
1151 Tsai, K., Thikmyanova, N., Wojcechowskyj, J.A., Delecluse, H.J., and Lieberman, P.M. (2011). EBV tegument
1152 protein BNRF1 disrupts DAXX-ATRX to activate viral early gene transcription. PLoS Pathog *7*, e1002376.

1153 Tsai, M.H., Raykova, A., Klinke, O., Bernhardt, K., Gartner, K., Leung, C.S., Geletneky, K., Sertel, S., Munz,
1154 C., Feederle, R.*, et al.* (2013). Spontaneous lytic replication and epitheliotropism define an Epstein-Barr
1155 virus strain found in carcinomas. Cell Rep *5*, 458-470.
1156 Uhlmann, F. (2016). SMC complexes: from DNA to chromosomes. Nat Rev Mol Cell Biol *17*, 399-412.
1157 Varshavsky, A. (2011). The N-end rule pathway and regulation by proteolysis. Protein Sci *20*, 1298-1345.
1158 Varshavsky, A. (2019). N-degron and C-degron pathways of protein degradation. Proc Natl Acad Sci U S A
1159 *116*, 358-366.
1160 Verma, D., Thompson, J., and Swaminathan, S. (2016). Spironolactone blocks Epstein-Barr virus
1161 production by inhibiting EBV SM protein function. Proc Natl Acad Sci U S A *113*, 3609-3614.
1162 Wang, I.X., Grunseich, C., Fox, J., Burdick, J., Zhu, Z., Ravazian, N., Hafner, M., and Cheung, V.G. (2018).
1163 Human proteins that interact with RNA/DNA hybrids. Genome Res *28*, 1405-1414.
1164 Wang, L.W., Shen, H., Nobre, L., Ersing, I., Paulo, J.A., Trudeau, S., Wang, Z., Smith, N.A., Ma, Y., Reinstadler,
1165 B.*, et al.* (2019a). Epstein-Barr-Virus-Induced One-Carbon Metabolism Drives B Cell Transformation. Cell
1166 Metab *30*, 539-555 e511.
1167 Wang, L.W., Wang, Z., Ersing, I., Nobre, L., Guo, R., Jiang, S., Trudeau, S., Zhao, B., Weekes, M.P., and
1168 Gewurz, B.E. (2019b). Epstein-Barr virus subverts mevalonate and fatty acid pathways to promote infected
1169 B-cell proliferation and survival. PLoS Pathog *15*, e1008030.
1170 Watt, J.L., Page, B.M., and Davidson, R.J. (1977). Cytogenetic study of 10 cases of infectious mononucleosis.
1171 Clin Genet *12*, 267-274.
1172 Wongsurawat, T., Gupta, A., Jenjaroenpun, P., Owens, S., Forrest, J.C., and Nookaew, I. (2020). R-loop-
1173 forming Sequences Analysis in Thousands of Viral Genomes Identify A New Common Element in
1174 Herpesviruses. Sci Rep *10*, 6389.
1175 Xu, W., Ma, C., Zhang, Q., Zhao, R., Hu, D., Zhang, X., Chen, J., Liu, F., Wu, K., Liu, Y.*, et al.* (2018). PJA1
1176 Coordinates with the SMC5/6 Complex To Restrict DNA Viruses and Episomal Genes in an Interferon-
1177 Independent Manner. J Virol *92*.
1178 Yu, Y., Li, S., Ser, Z., Sanyal, T., Choi, K., Wan, B., Kuang, H., Sali, A., Kentsis, A., Patel, D.J.*, et al.* (2021).
1179 Integrative analysis reveals unique structural and functional features of the Smc5/6 complex. Proc Natl
1180 Acad Sci U S A *118*.
1181 Zur Hausen, H., and de Villiers, E.M. (2015). Reprint of: cancer "causation" by infections--individual
1182 contributions and synergistic networks. Semin Oncol *42*, 207-222.

1183

Figure 1

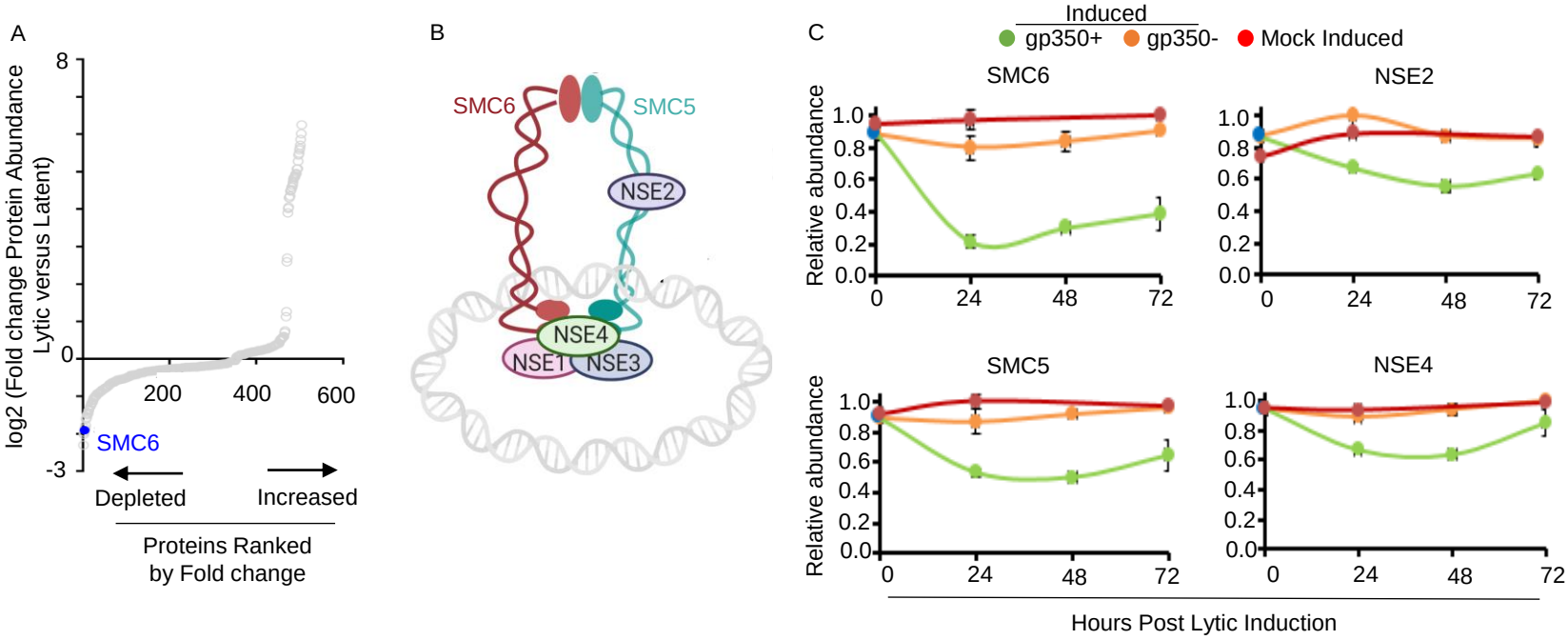
A
log2 (Fold change Protein Abundance Lytic versus Latent)
8
0
-3
200
400
600
SMC6
Depleted
Increased
Proteins Ranked by Fold change
B
SMC6
SMC5
NSE2
NSE4
NSE1
NSE3
C
Induced
gp350+
gp350-
Mock Induced
SMC6
NSE2
SMC5
NSE4
Relative abundance
1.0
0.8
0.6
0.4
0.2
0.0
0
24
48
72
Hours Post Lytic Induction

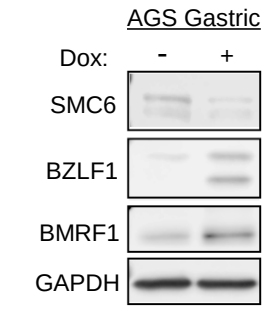
D
AGS Gastric
Dox:
-
+
SMC6
BZLF1
BMRF1
GAPDH

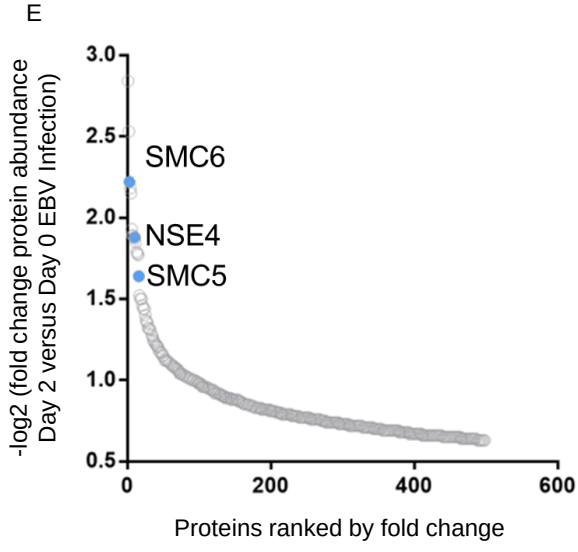
E
-log2 (fold change protein abundance Day 2 versus Day 0 EBV Infection)
3.0
2.5
2.0
1.5
1.0
0.5
SMC6
NSE4
SMC5
0
200
400
600
Proteins ranked by fold change

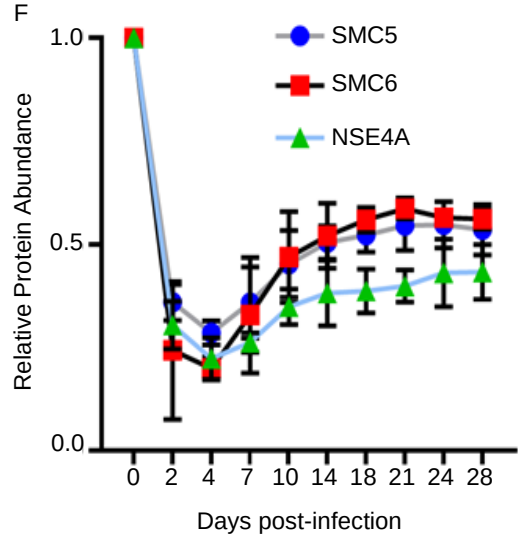
F
Relative Protein Abundance
1.0
0.5
0.0
SMC5
SMC6
NSE4A
0
2
4
7
10
14
18
21
24
28
Days post-infection

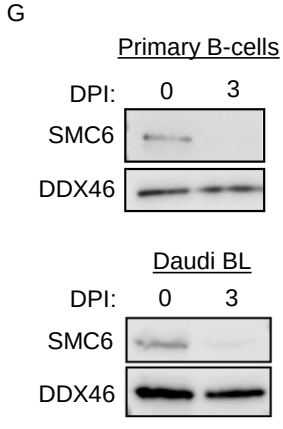
G
Primary B-cells
DPI:
0
3
SMC6
DDX46
Daudi BL
DPI:
0
3
SMC6
DDX46

Figure 2

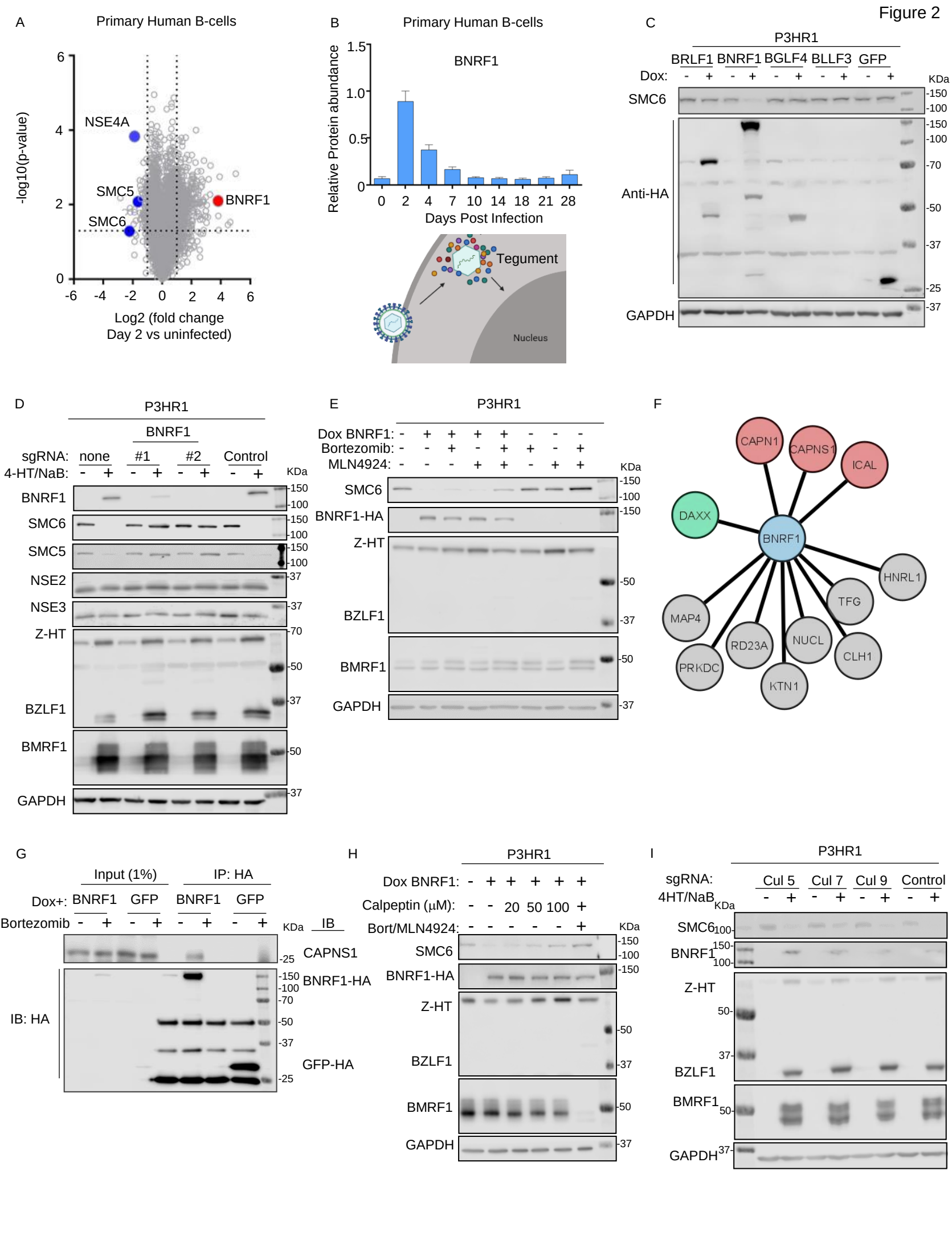
A
Primary Human B-cells
-log10(p-value)
NSE4A
SMC5
SMC6
BNRF1
Log2 (fold change
Day 2 vs uninfected)
B
Primary Human B-cells
BNRF1
Relative Protein abundance
Days Post Infection
Tegument
Nucleus
C
P3HR1
BRLF1 BNRF1 BGLF4 BLLF3 GFP
Dox:
KDa
SMC6
Anti-HA
GAPDH
D
P3HR1
BNRF1
sgRNA: none #1 #2 Control
4-HT/NaB:
BNRF1
SMC6
SMC5
NSE2
NSE3
Z-HT
BZLF1
BMRF1
GAPDH
E
P3HR1
Dox BNRF1:
Bortezomib:
MLN4924:
SMC6
BNRF1-HA
Z-HT
BZLF1
BMRF1
GAPDH
F
CAPN1
CAPNS1
ICAL
DAXX
BNRF1
HNRL1
TFG
MAP4
RD23A
NUCL
CLH1
PRKDC
KTN1
G
Input (1%)
IP: HA
Dox+:
BNRF1 GFP BNRF1 GFP
Bortezomib
IB
CAPNS1
BNRF1-HA
IB: HA
GFP-HA
H
P3HR1
Dox BNRF1:
Calpeptin (μM): 20 50 100
Bort/MLN4924:
SMC6
BNRF1-HA
Z-HT
BZLF1
BMRF1
GAPDH
I
P3HR1
sgRNA: Cul 5 Cul 7 Cul 9 Control
4HT/NaB
SMC6
BNRF1
Z-HT
BZLF1
BMRF1
GAPDH

Figure 3

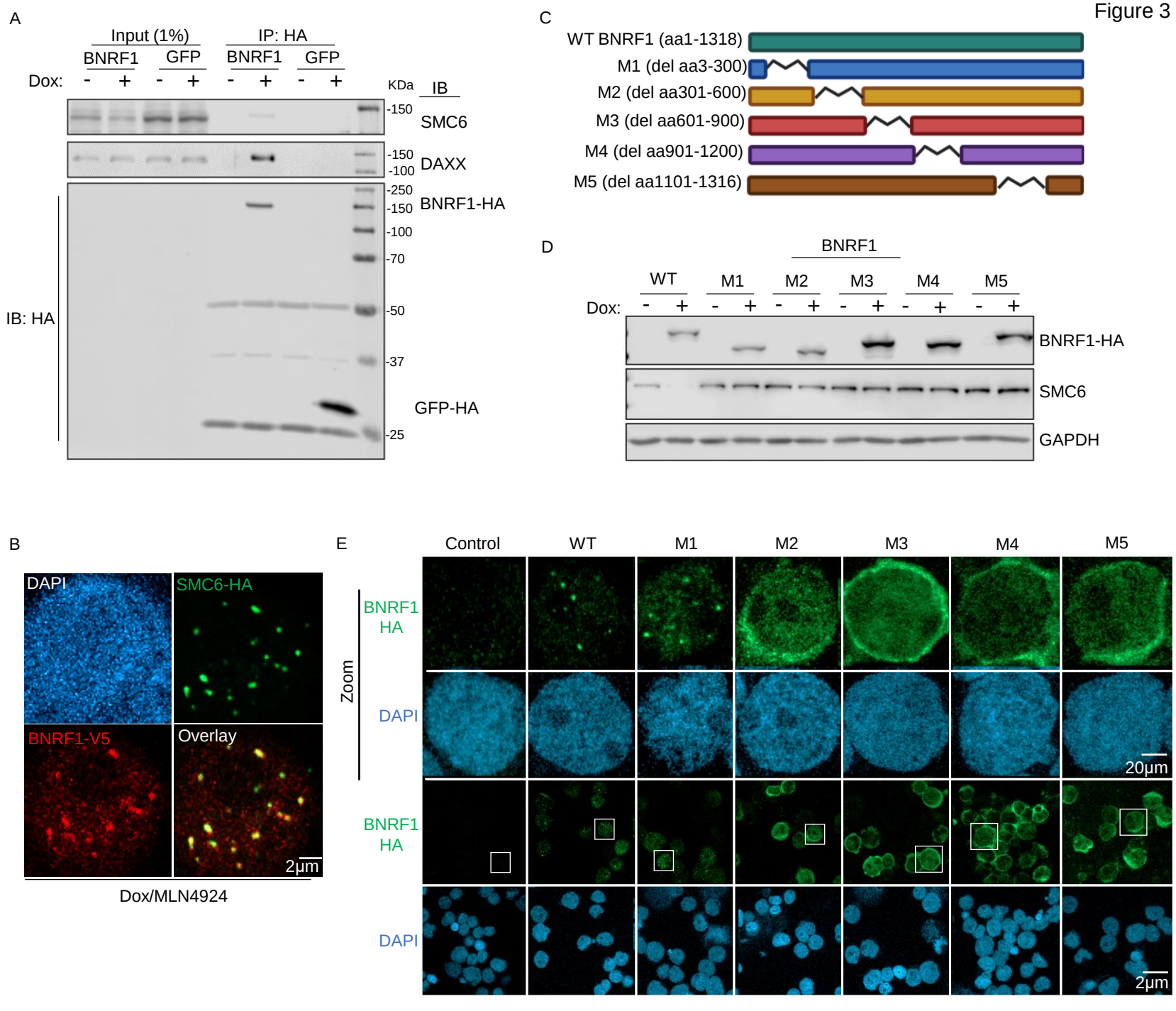
A
Input (1%)
IP: HA
BNRF1
GFP
BNRF1
GFP
Dox:
- + - + - + - +
KDa
IB
-150
SMC6
-150
-100
DAXX
-250
-150
BNRF1-HA
-100
-70
IB: HA
-50
-37
GFP-HA
-25
C
WT BNRF1 (aa1-1318)
M1 (del aa3-300)
M2 (del aa301-600)
M3 (del aa601-900)
M4 (del aa901-1200)
M5 (del aa1101-1316)
D
BNRF1
WT
M1
M2
M3
M4
M5
Dox:
- + - + - + - + - + - +
BNRF1-HA
SMC6
GAPDH
B
DAPI
SMC6-HA
BNRF1-V5
Overlay
2μm
Dox/MLN4924
E
Control
WT
M1
M2
M3
M4
M5
Zoom
BNRF1 HA
DAPI
20μm
BNRF1 HA
DAPI
2μm

Figure 4

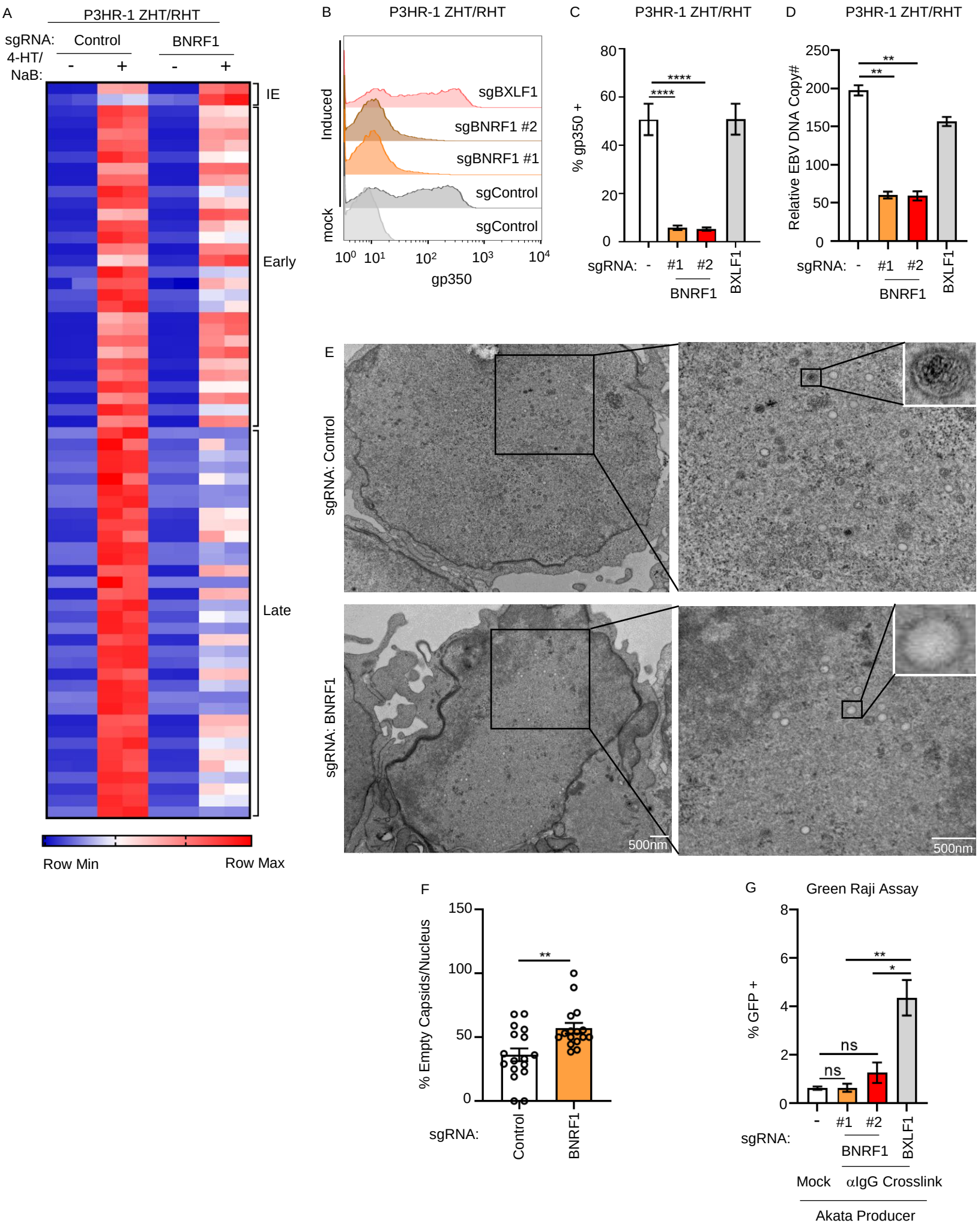
A
P3HR-1 ZHT/RHT
sgRNA:
Control
BNRF1
4-HT/
NaB:
-
+
-
+
IE
Early
Late
Row Min
Row Max
B
P3HR-1 ZHT/RHT
Induced
mock
sgBXLF1
sgBNRF1 #2
sgBNRF1 #1
sgControl
sgControl
gp350
C
P3HR-1 ZHT/RHT
% gp350 +
sgRNA:
#1
#2
BNRF1
BXLF1
D
P3HR-1 ZHT/RHT
Relative EBV DNA Copy#
sgRNA:
#1
#2
BNRF1
BXLF1
E
sgRNA: Control
sgRNA: BNRF1
500nm
500nm
F
% Empty Capsids/Nucleus
sgRNA:
Control
BNRF1
G
Green Raji Assay
% GFP +
sgRNA:
#1
#2
BNRF1
BXLF1
Mock
αIgG Crosslink
Akata Producer

Figure 5

A

BNRF1

sgRNA: None #1 #2 BXLF1

BMRF1 EdC Overlay

Zoom

20μm

2μm

P3HR1 +4HT/NaB

B

10mm

sgControl

sgBNRF1

C

% of P3HR1 nuclei with RC

****

sgRNA: Control BNRF1 BXLF1

D

sgRNA: None sgControl sgBNRF1 BNRF1^{R}-cDNA + sgBNRF1

BMRF1 EdC Overlay

Zoom

20μm

2μm

Mock induced

P3HR1 +4-HT/NaB

E

10mm

sgBNRF1

BNRF1^{R}-cDNA + sgBNRF1

F

% of Akata nuclei with RC

**

***

sgRNA: - - BNRF1 BNRF1

BNRF1-cDNA: - - - +

Mock 4HT/NaB

G

Bortezomib (5nM)

sgRNA: None None SMC6 Control

BMRF1 EdC Overlay

Zoom

20μm

2μm

P3HR1 +4HT/NaB

H

10mm

sgControl +Bortezomib

sgSMC6 +Bortezomib

I

% of nucleiP3HR1 with RC

****

****

sgRNA: None None SMC6 Control

Bortezomib: - + - +

J

sgRNA: None BNRF1 BXLF1 BNRF1/ SMC6

BMRF1 EdC Overlay

Zoom

20μm

2μm

EBV+ Akata αIgG Crosslink

K

10mm

sgBNRF1

sgBNRF1/ SMC6

L

% of Akata nuclei with RC

****

***

sgRNA: Control BNRF1 BXLF1 BNRF1/ SMC6

Figure 6

A

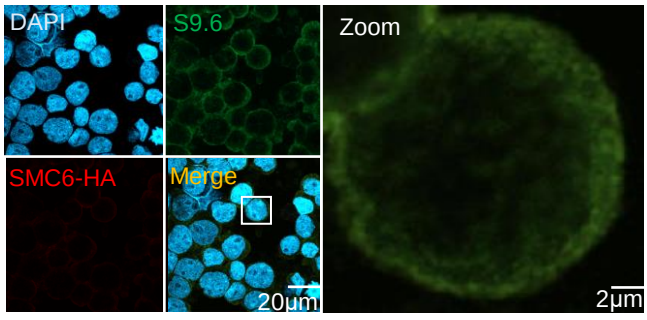

- Dox (SMC6-HA), - 4-HT/NaB (latent)

B

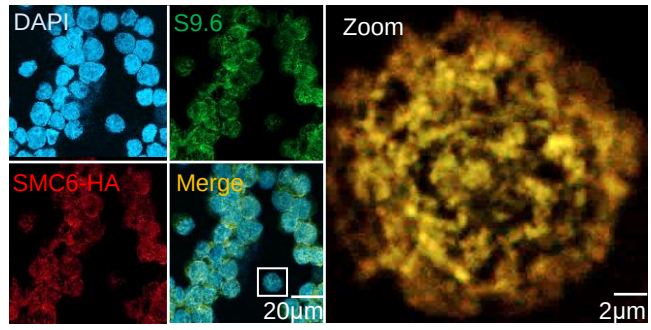

+Dox (SMC6-HA), +4-HT/NaB (Lytic)

C

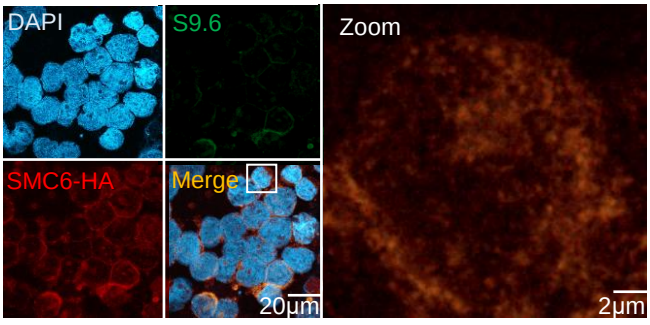

+Dox (SMC6-HA), +4-HT/NaB (Lytic) + RNase H

F

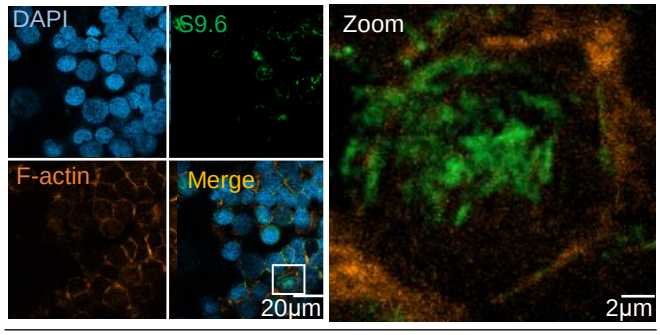

+Dox SMC6-HA, +4-HT/NaB Lytic

D

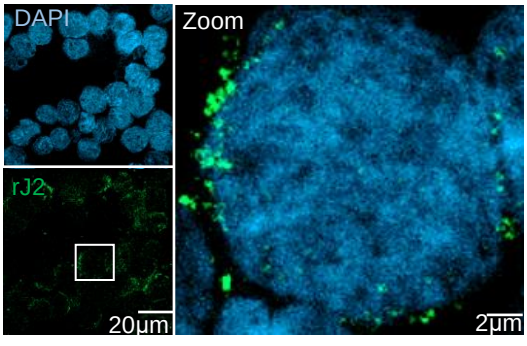

+Dox (SMC6-HA), +4-HT/NaB (Lytic)

G

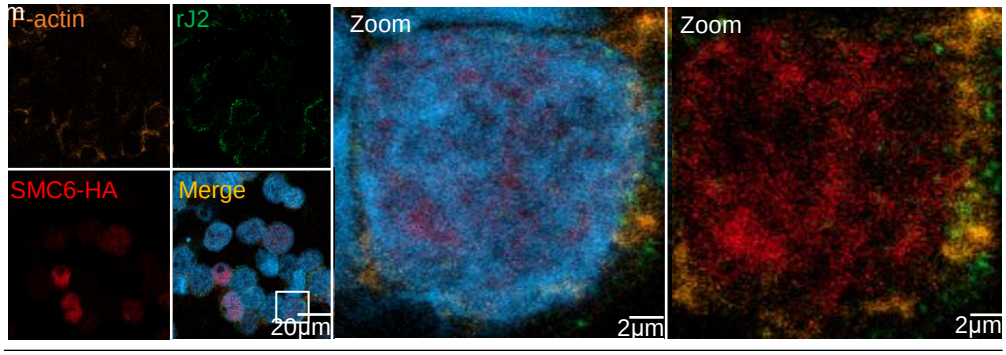

+Dox (SMC6-HA), +4-HT/NaB (Lytic)

E

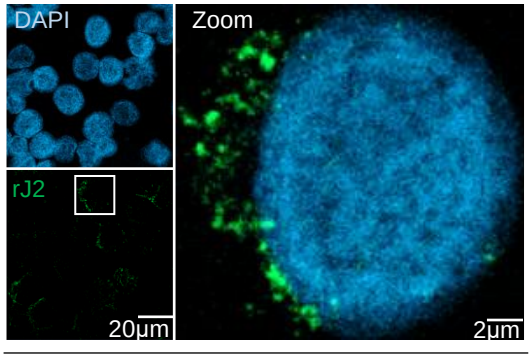

+Dox (SMC6-HA), +4-HT/NaB (Lytic) + RNaseH

H

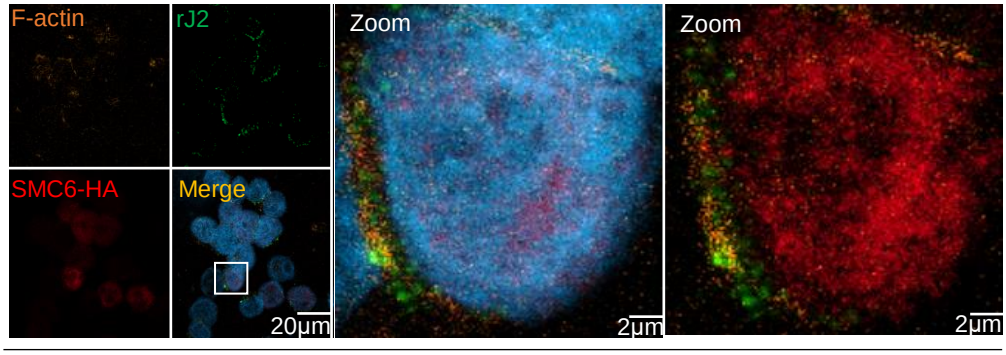

+Dox (SMC6-HA), +4-HT/NaB (Lytic) + RNaseH

I

	Input					IP:S9.6				
4-HT/NaB/Dox	-	+	+	+	+	-	+	+	+	+
RNaseH	-	+	-	-	-	-	+	-	-	-
Benzonase	-	-	-	+	-	-	-	-	+	-
PAA	-	-	-	-	+	-	-	-	-	+

IP:S9.6

HA-SMC6

J

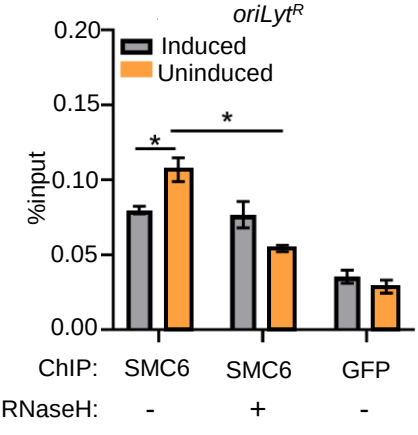

Figure 7

A

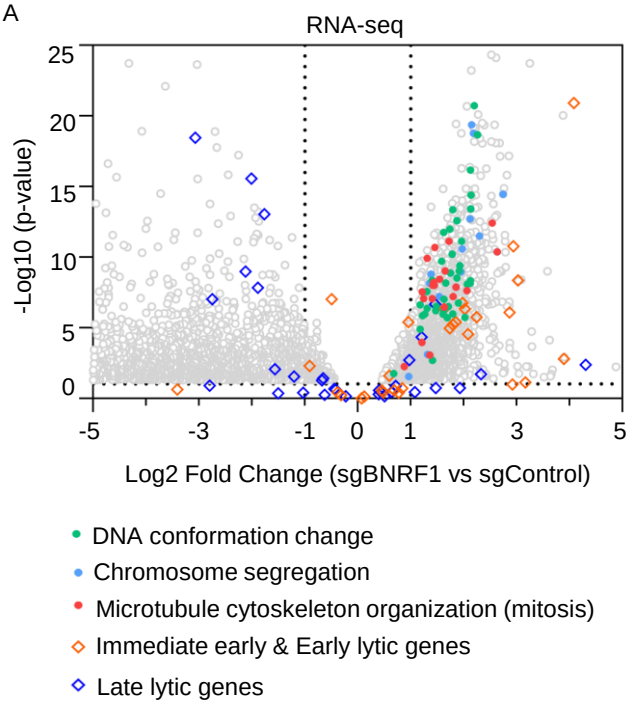
RNA-seq
-Log10 (p-value)
25
20
15
10
5
0
-5
-3
-1
0
1
3
5
Log2 Fold Change (sgBNRF1 vs sgControl)
DNA conformation change
Chromosome segregation
Microtubule cytoskeleton organization (mitosis)
Immediate early & Early lytic genes
Late lytic genes

B

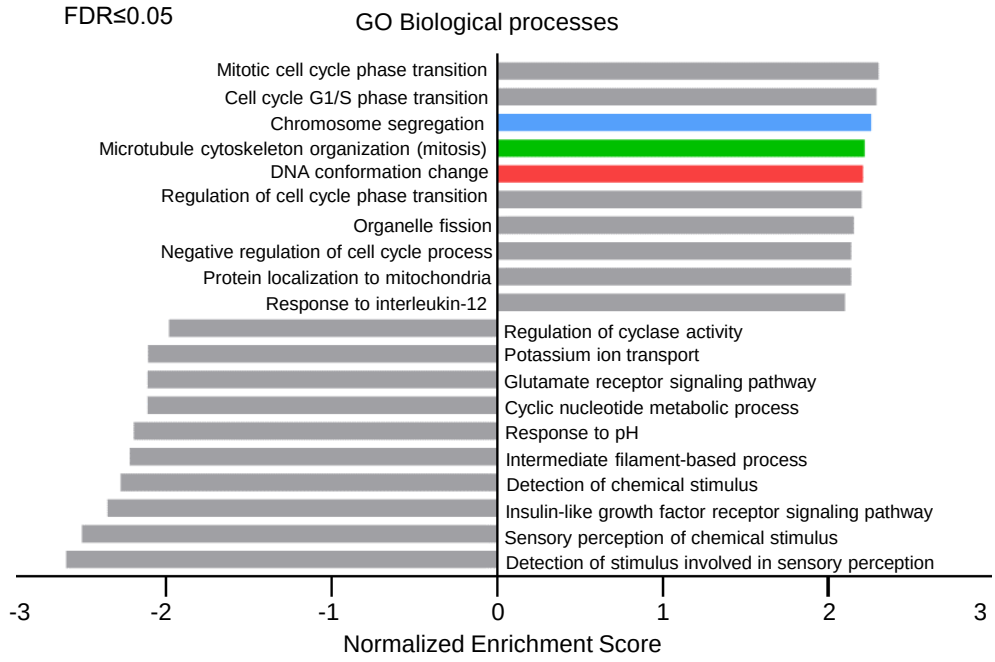
FDR≤0.05
GO Biological processes
Mitotic cell cycle phase transition
Cell cycle G1/S phase transition
Chromosome segregation
Microtubule cytoskeleton organization (mitosis)
DNA conformation change
Regulation of cell cycle phase transition
Organelle fission
Negative regulation of cell cycle process
Protein localization to mitochondria
Response to interleukin-12
Regulation of cyclase activity
Potassium ion transport
Glutamate receptor signaling pathway
Cyclic nucleotide metabolic process
Response to pH
Intermediate filament-based process
Detection of chemical stimulus
Insulin-like growth factor receptor signaling pathway
Sensory perception of chemical stimulus
Detection of stimulus involved in sensory perception
-3
-2
-1
0
1
2
3
Normalized Enrichment Score

C

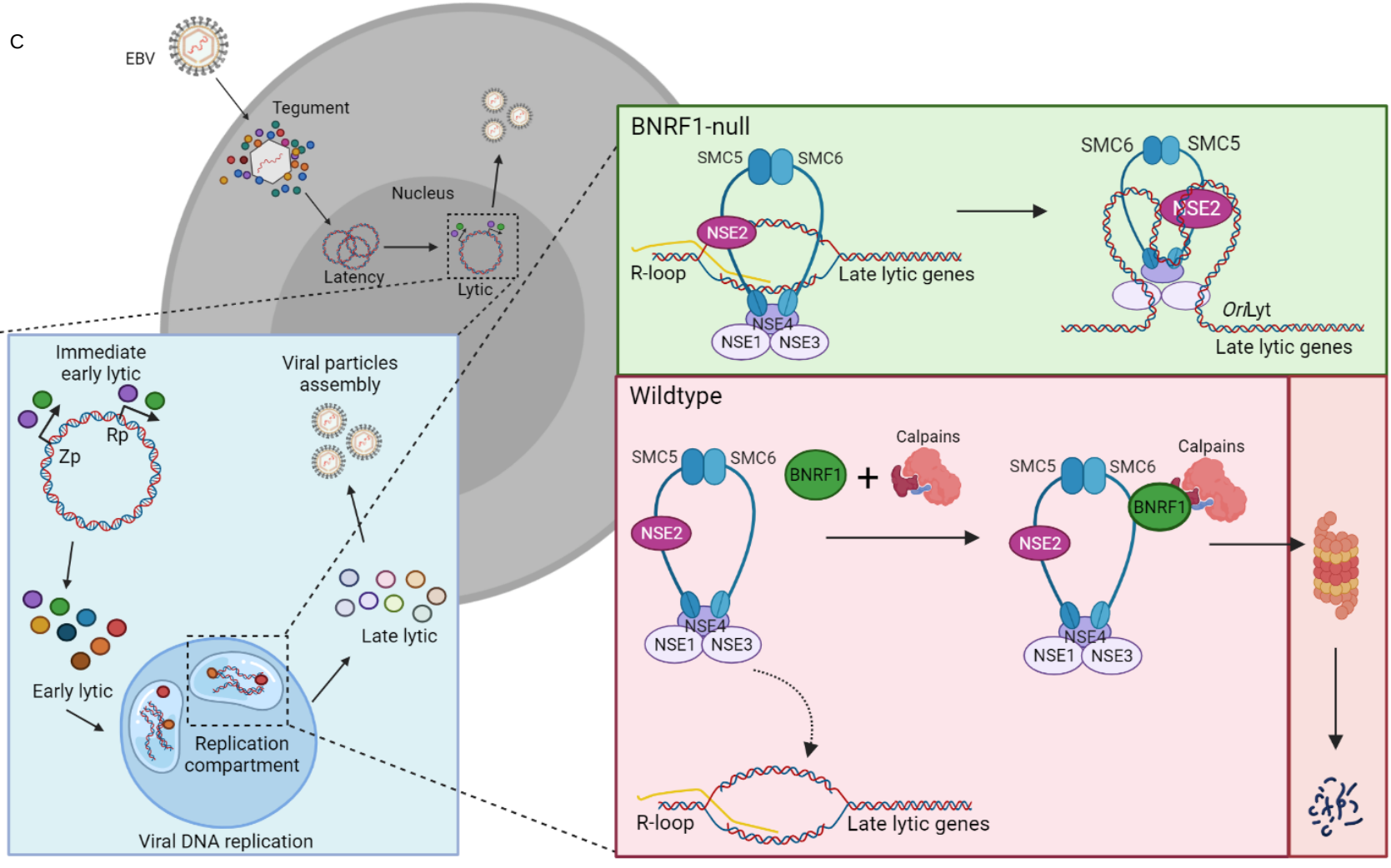
EBV
Tegument
Nucleus
Latency
Lytic
Immediate early lytic
Viral particles assembly
Rp
Zp
Early lytic
Late lytic
Replication compartment
Viral DNA replication
BNRF1-null
SMC5
SMC6
NSE2
R-loop
Late lytic genes
NSE4
NSE1
NSE3
OriLyt
Wildtype
BNRF1
Calpains
R-loop

Figure S1

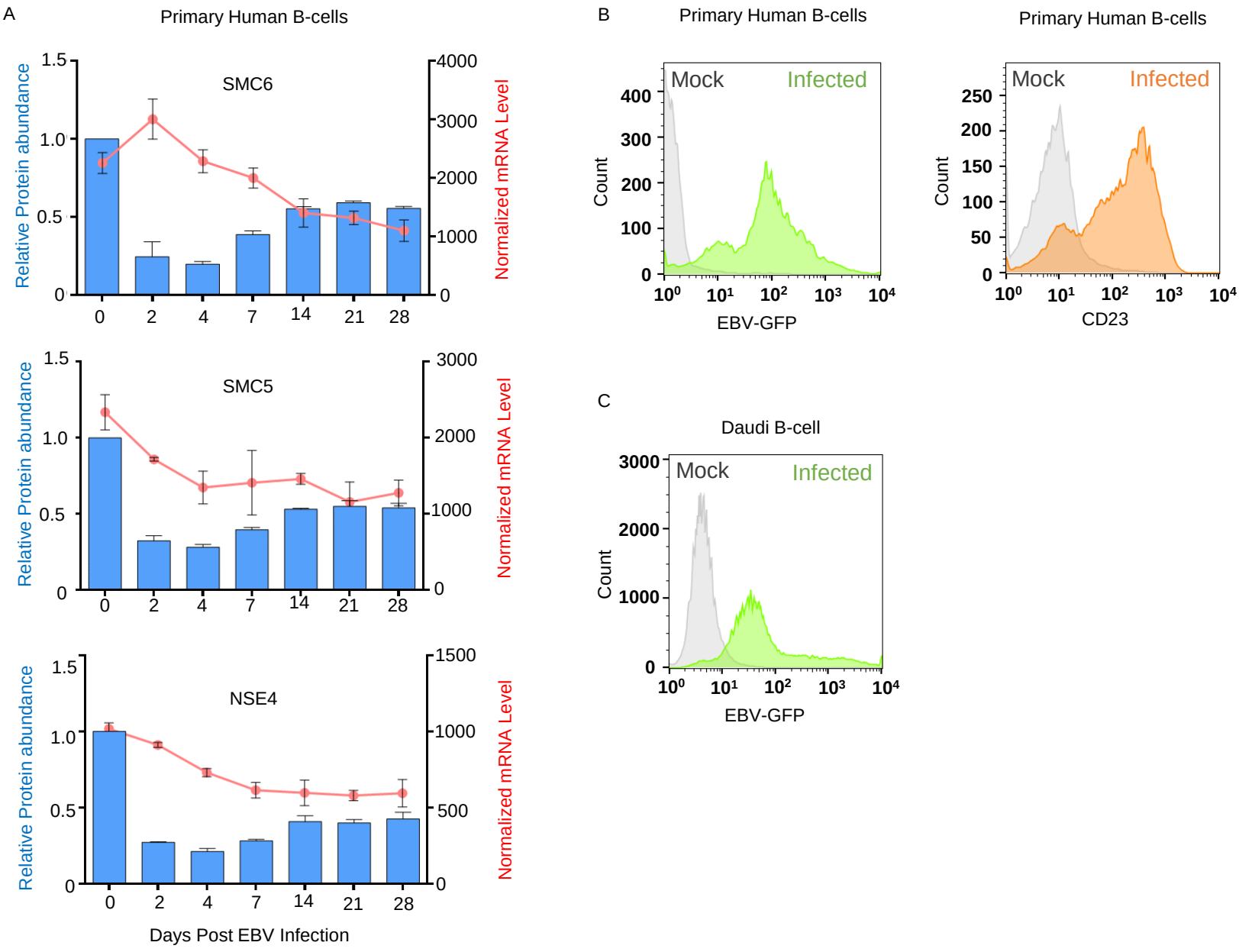
A
Primary Human B-cells
SMC6
SMC5
NSE4
Relative Protein abundance
Normalized mRNA Level
Days Post EBV Infection
B
Primary Human B-cells
Mock
Infected
Count
EBV-GFP
CD23
C
Daudi B-cell

Figure S2

A

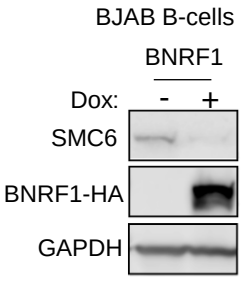

B

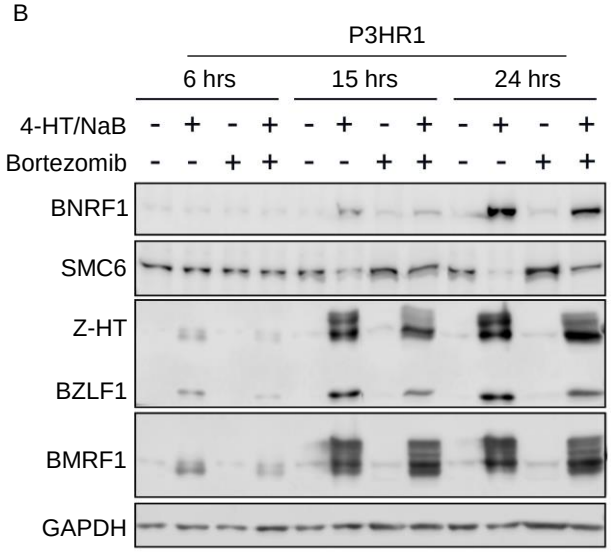

C

Bait	Prey	Z-score
BNRF1	KTN1	2.67
	CAPNS1	2.67
	DAXX	2.66
	ICAL	2.64
	CAPN1	2.61
	RD23A	2.61
	PKRDC	1.53
	MAP4	1.36
	NUCL	1.10
	HNRF1	1.03
	CLH1	0.97
	TFG	0.81

D

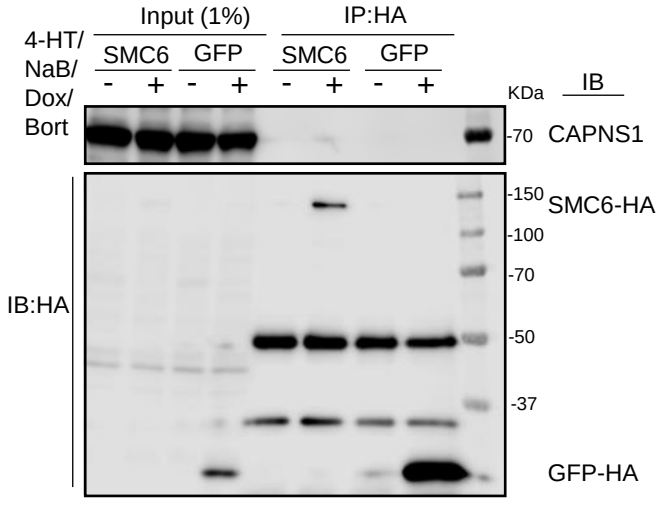

E

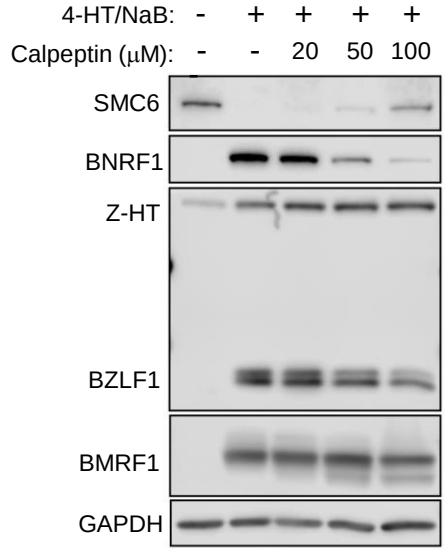

F

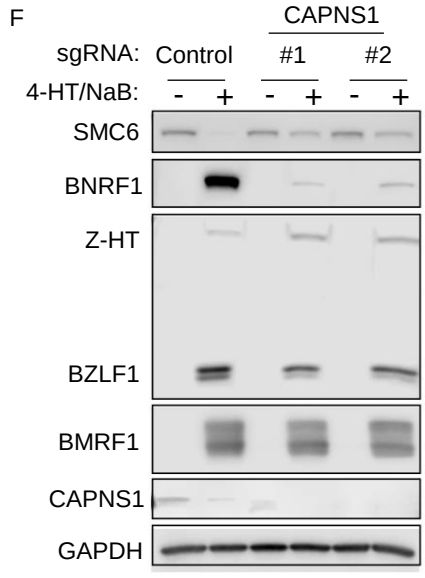

G

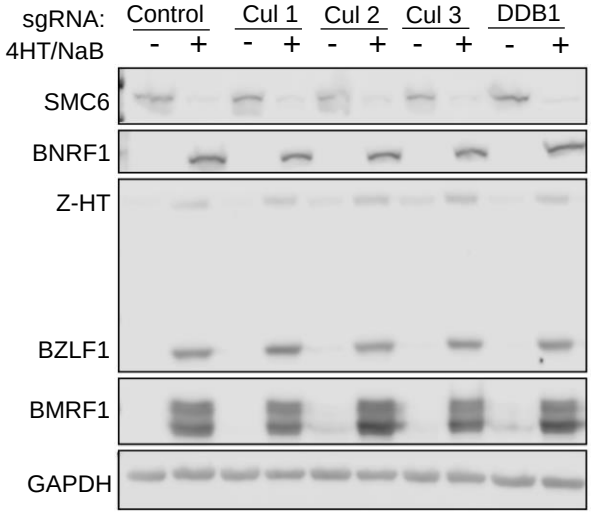

H

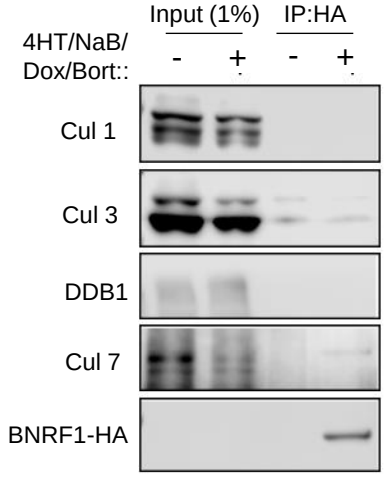

I

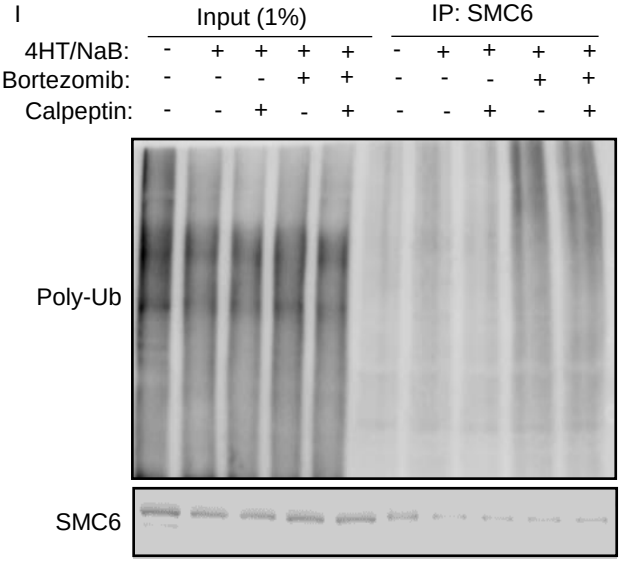

Figure S3

A

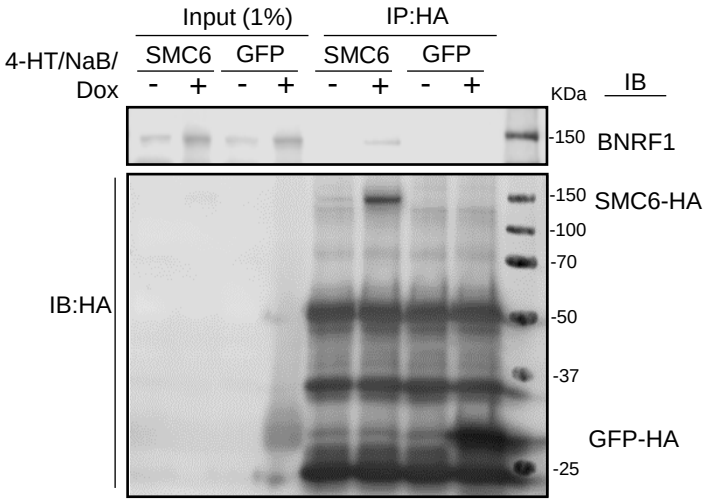

B

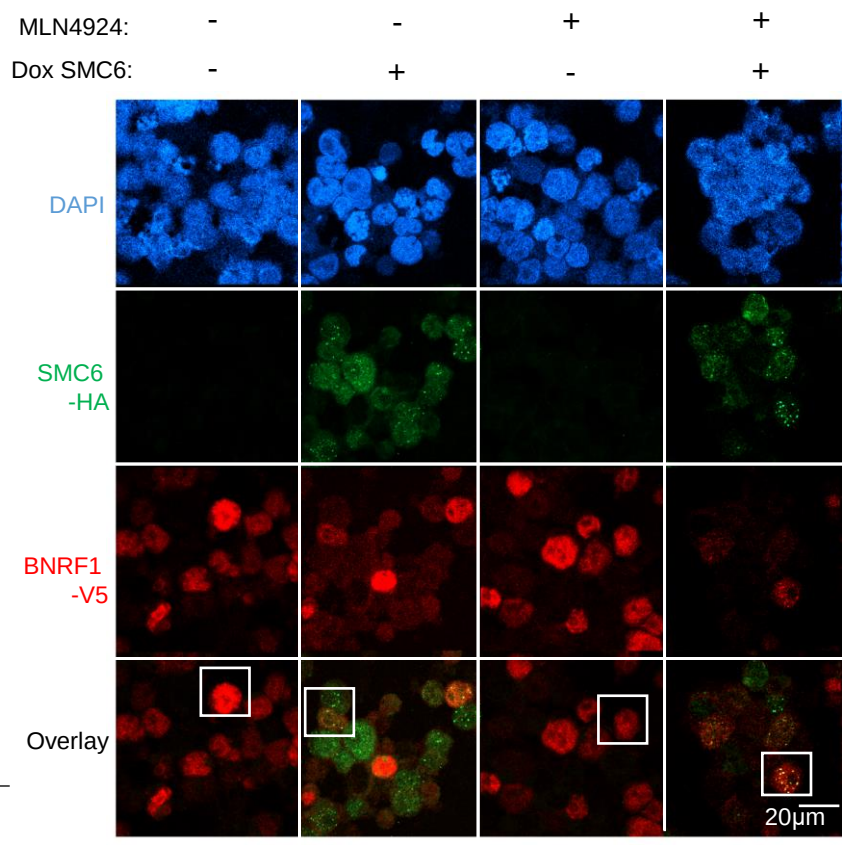

C

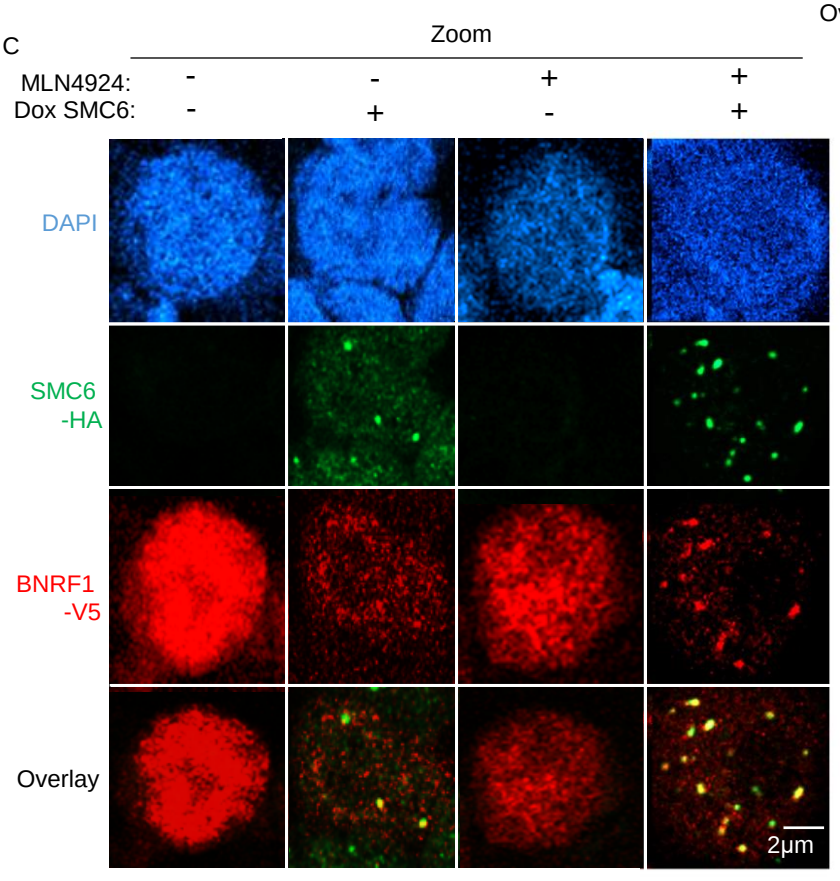

D

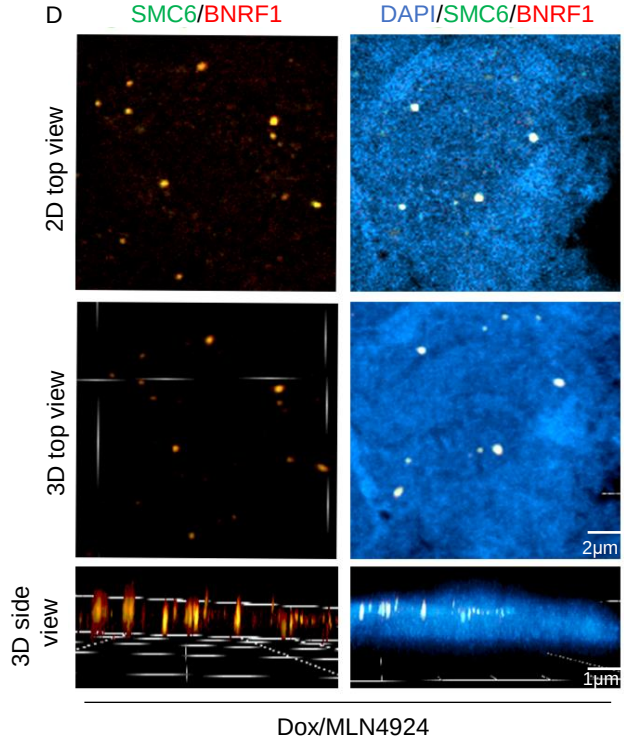

E

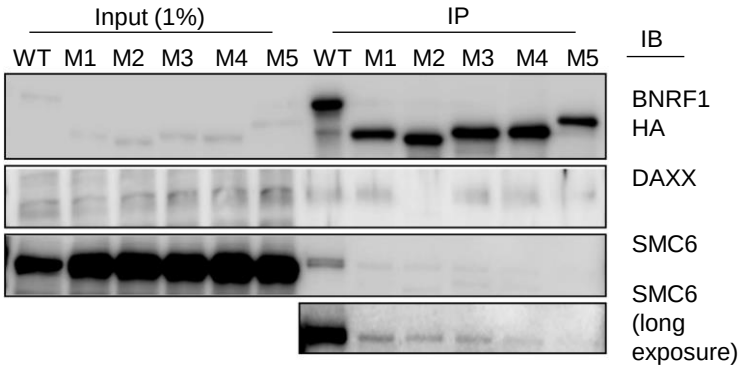

Figure S4

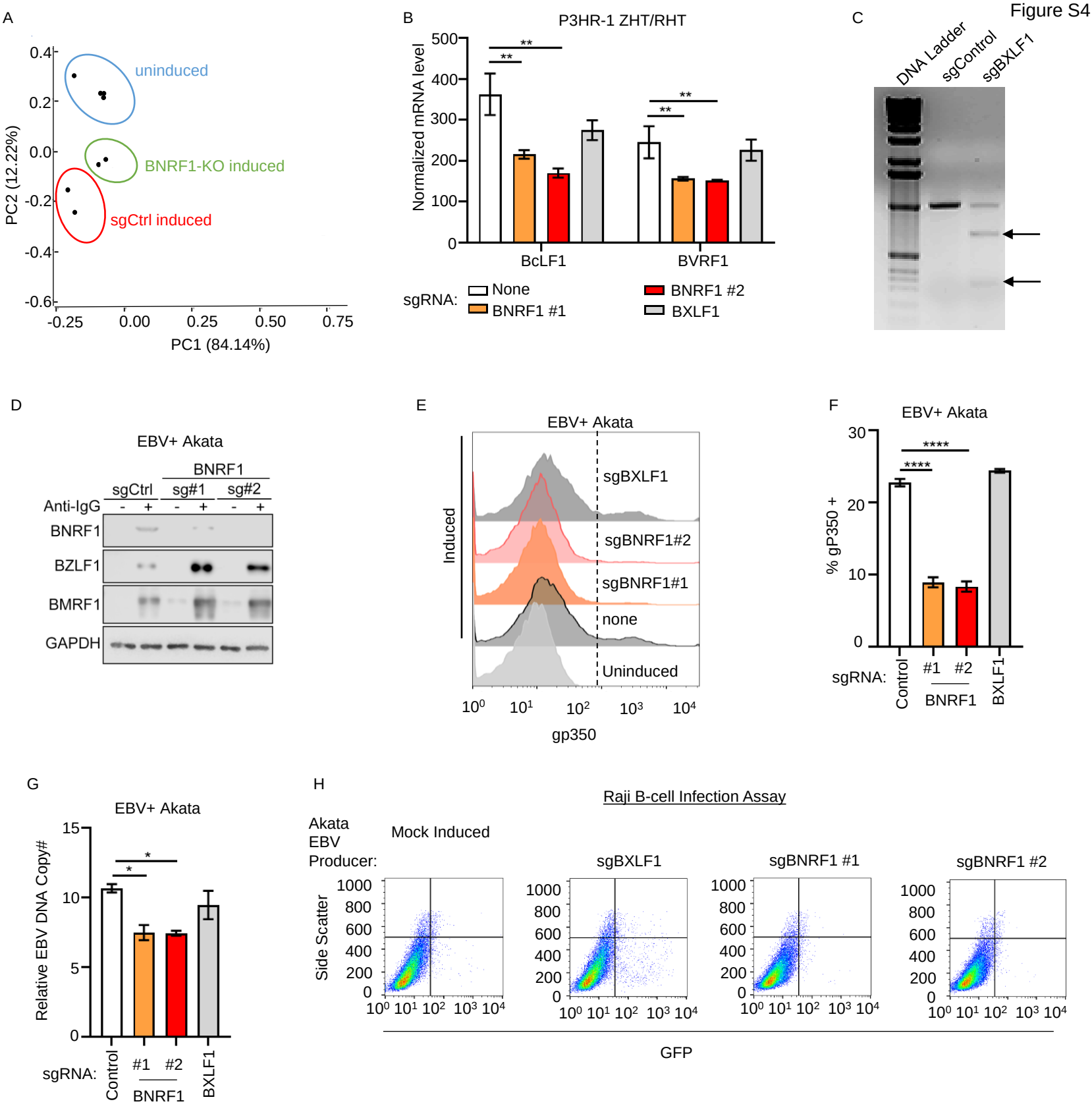
A
uninduced
BNRF1-KO induced
sgCtrl induced
PC2 (12.22%)
PC1 (84.14%)
B
P3HR-1 ZHT/RHT
Normalized mRNA level
BcLF1
BVRF1
sgRNA:
None
BNRF1 #1
BNRF1 #2
BXLF1
C
DNA Ladder
sgControl
sgBXLF1
D
EBV+ Akata
BNRF1
sgCtrl
sg#1
sg#2
Anti-IgG
BNRF1
BZLF1
BMRF1
GAPDH
E
EBV+ Akata
Induced
sgBXLF1
sgBNRF1#2
sgBNRF1#1
none
Uninduced
gp350
F
EBV+ Akata
% gP350 +
sgRNA:
Control
#1
#2
BNRF1
BXLF1
G
EBV+ Akata
Relative EBV DNA Copy#
sgRNA:
Control
#1
#2
BNRF1
BXLF1
H
Raji B-cell Infection Assay
Akata EBV Producer:
Mock Induced
sgBXLF1
sgBNRF1 #1
sgBNRF1 #2
Side Scatter
GFP

Figure S5

A

sgRNA: Control | BNRF1 #1 | BNRF1 #2 | BXLF1

DAPI

BMRF1

EdC

Overlay

Zoom

20μm

2μm

P3HR1 +4HT/NaB

B

sgRNA: BXLF1 | BNRF1

DAPI

BMRF1

EdC

Overlay

2μm

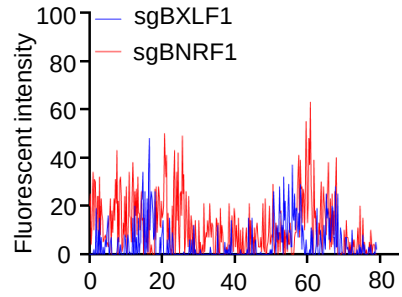

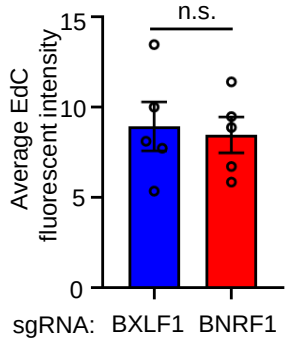

C

BMRF1/EdC | DAPI/BMRF1/EdC

2D top view

3D top view

3D side view

2μm

1μm

P3HR1 +4HT/NaB

D

sgRNA: Uninduced | Control | sgBNRF1 | BNRF1-cDNA^R sgBNRF1

DAPI

BMRF1

EdC

Overlay

Zoom

20μm

2μm

EBV+ Akata αIgG Crosslink

E

sgRNA: BNRF1 | Control

αIgG: - + - +

BNRF1-V5

BNRF1

BZLF1

BMRF1

GAPDH

Figure S6

A

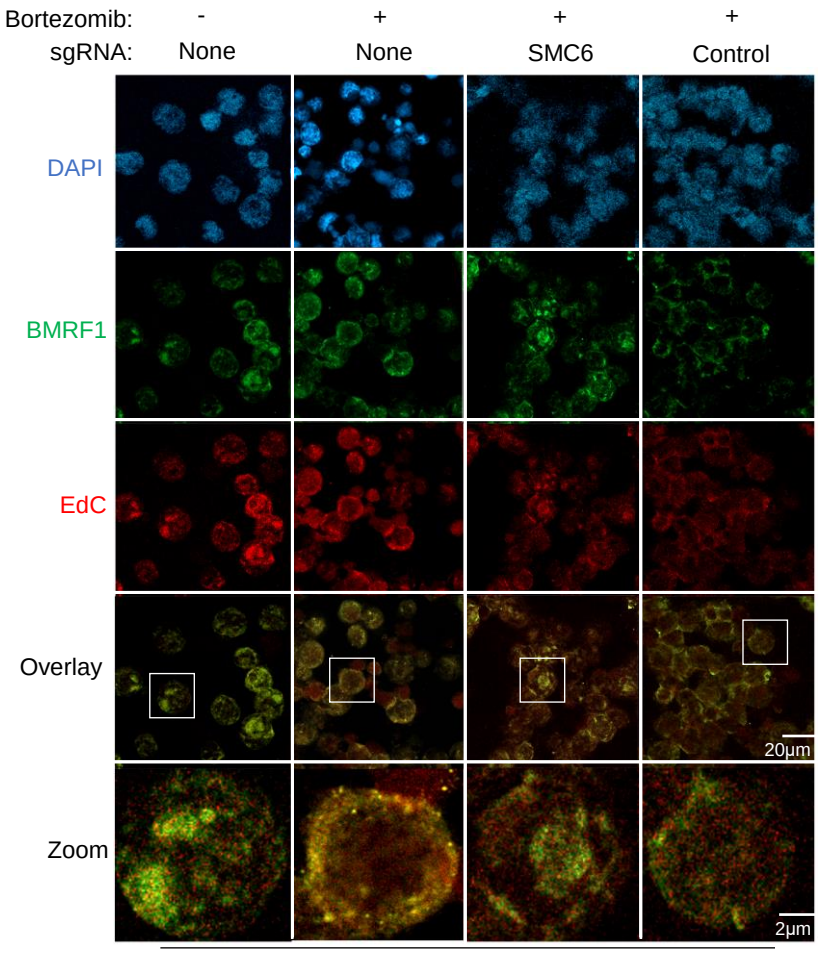

P3HR1 +4HT/NaB

B

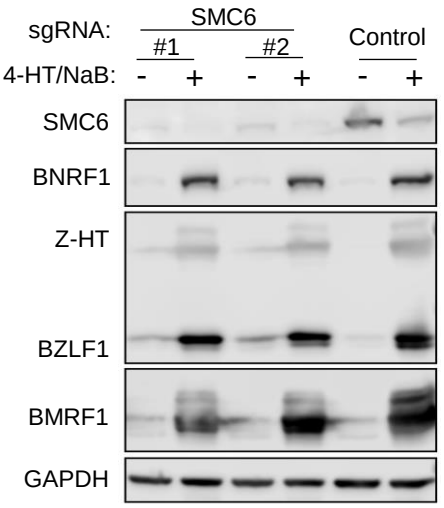

D

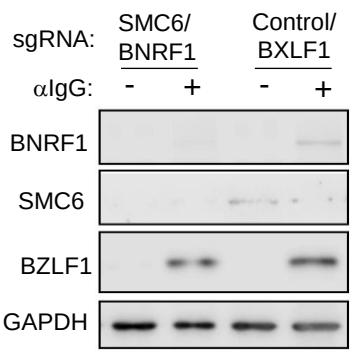

E

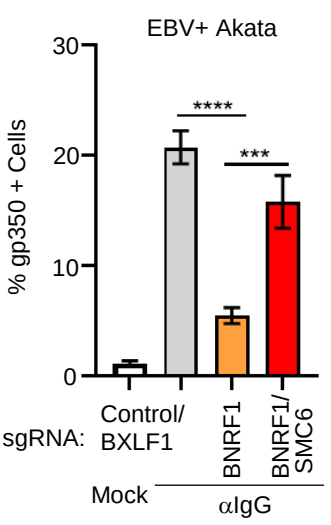

F

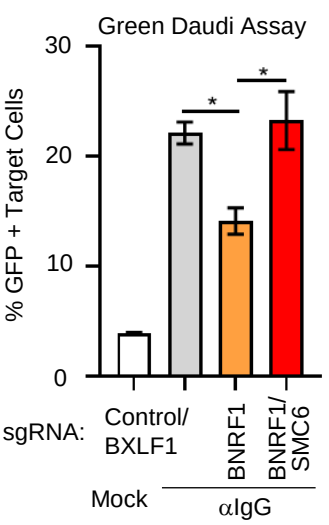

C

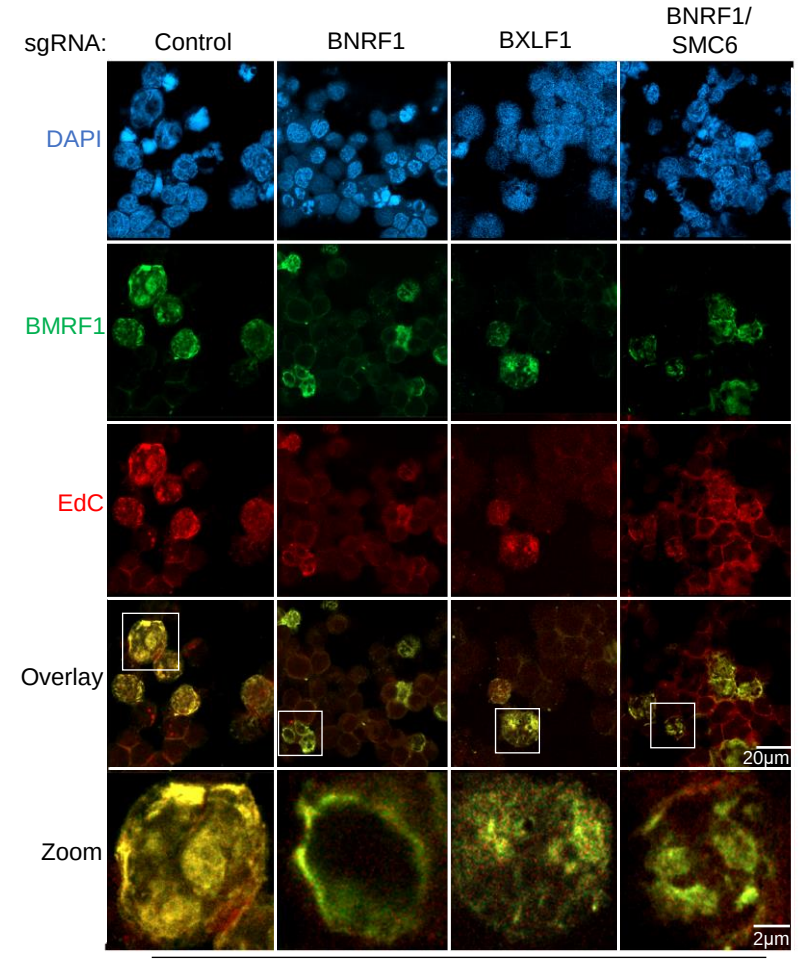

EBV+ Akata αIgG Crosslink

G

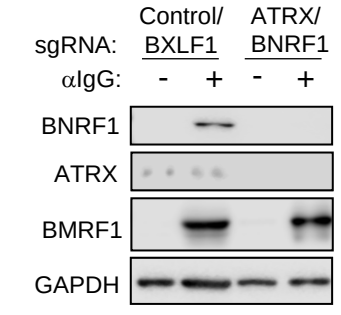

H

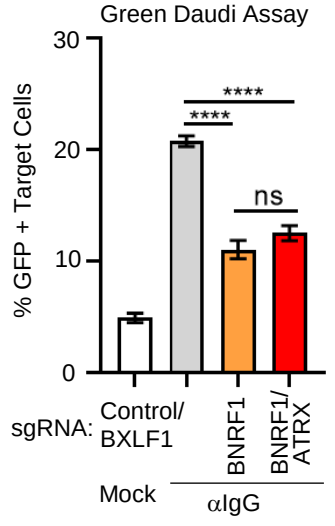

Figure S7

A

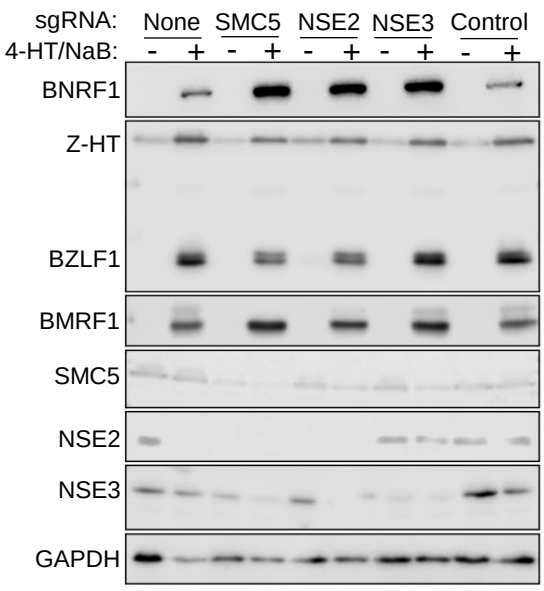

B

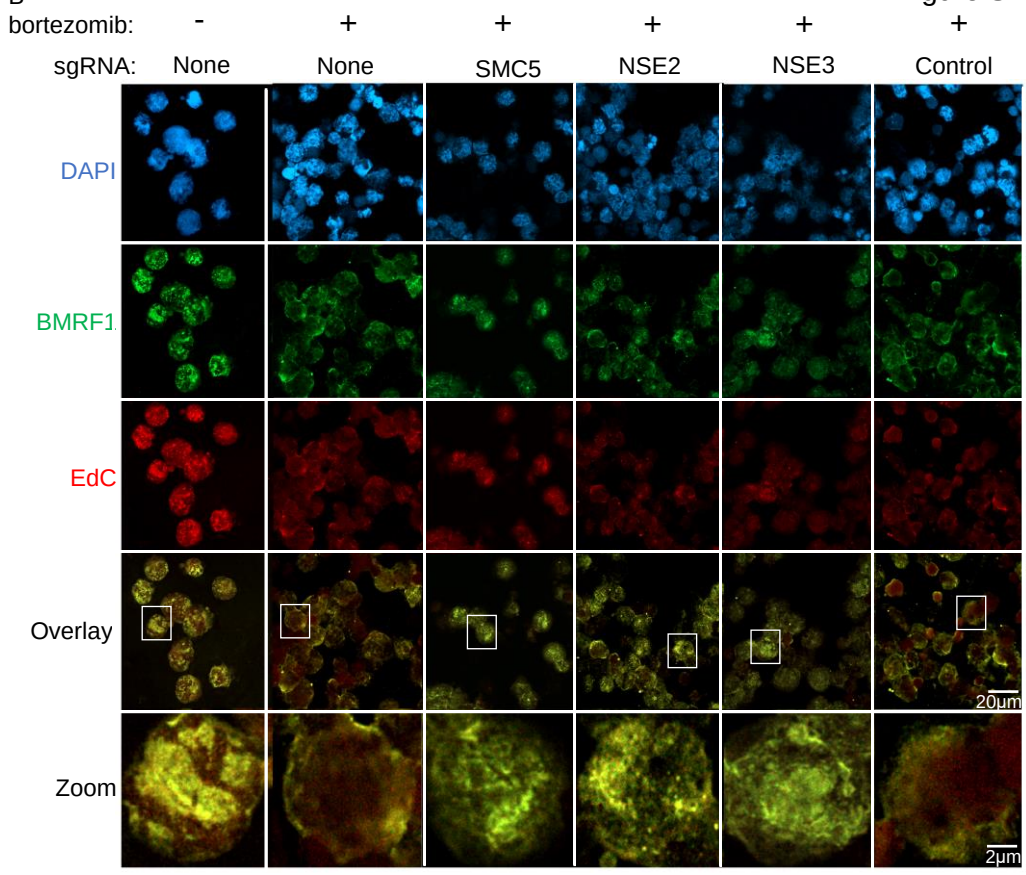

P3HR1 ZHT/RHT

C

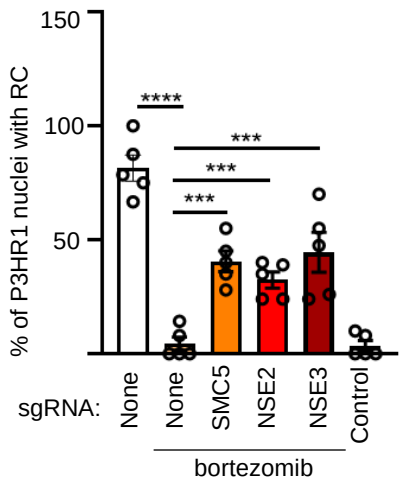

D

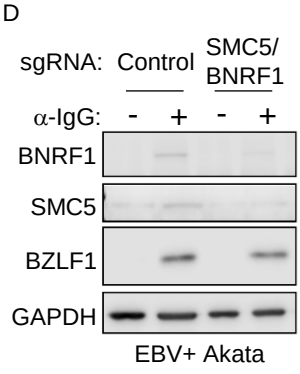

E

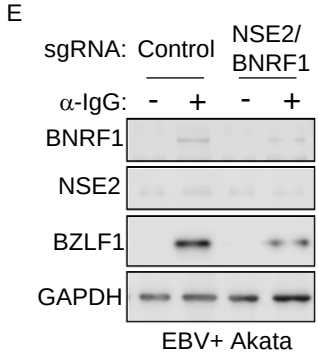

F

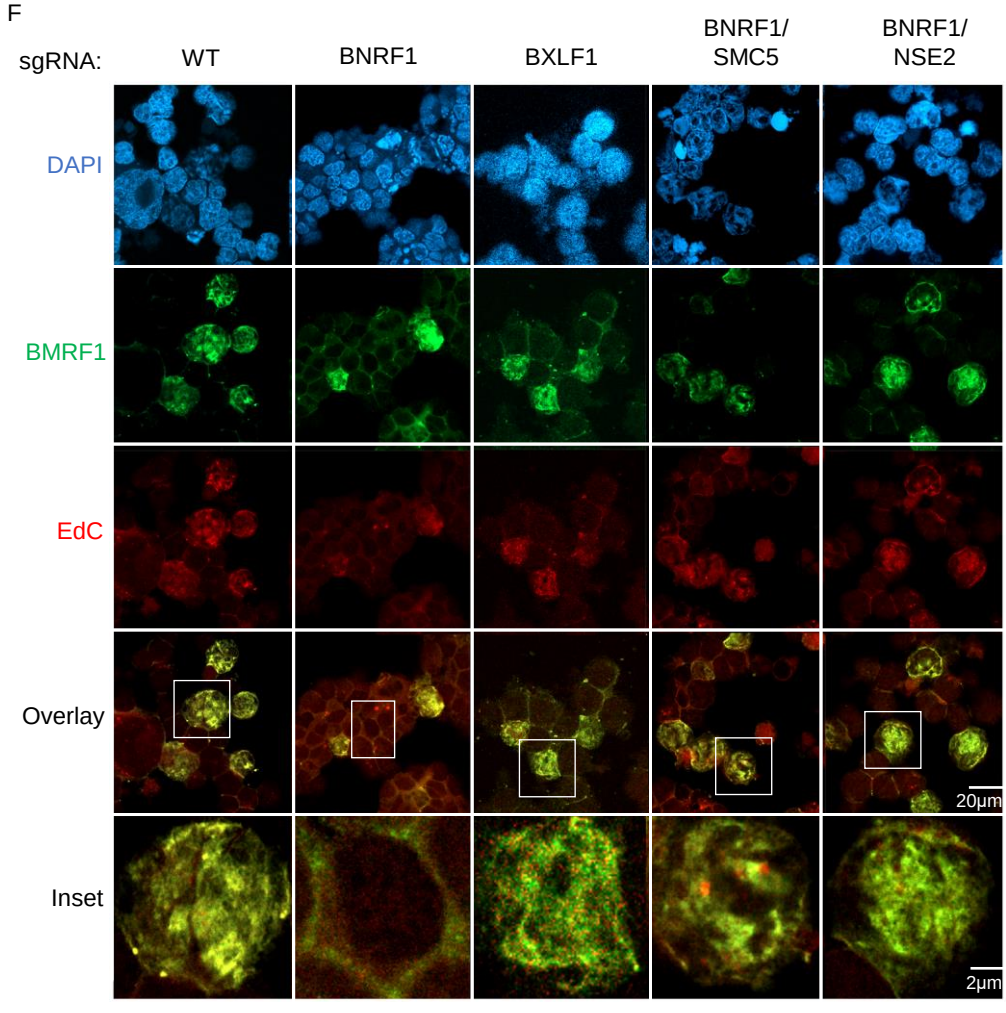

EBV+ Akata

G

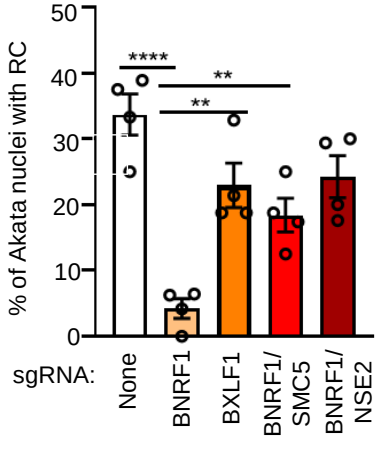

Supplementary Figures:

Figure S1. Related to Figure 1: the SMC5/6 cohesin complex is depleted by incoming EBV.

(A) Relative protein abundances (blue) and normalized mRNA levels (red) of SMC6, SMC5 and NSE4 at the indicated days post infection of primary human B-cells. SEM values from n=4 proteomic and n=3 RNA-seq replicates are shown. Data are from (Ersing et al., 2017; Wang et al., 2019a).

(B) FACS analysis of GFP levels (left) and CD23 levels (right) in primary human B-cells mock infected or infected by Akata GFP+ EBV at 48 hours post-infection (hpi). GFP and CD23 upregulation were used as markers of EBV infection.

(C) FACS analysis of GFP levels in Daudi cells super-infected by Akata GFP+ EBV at 48 hpi.

Figure S2. Related to Figure 2: BNRF1 targets SMC5/6 for proteasomal degradation in a calpain-and cullin-dependent manner.

(A) WCL of EBV- BJAB B-cells mock or doxycycline induced for BNRF1 expression for 24 hours.

(B) Immunoblot analysis of WCL from P3HR-1 ZHT/RHT cells induced for lytic replication and treated with bortezomib as indicated.

(C) Table of high confidence host proteins interactors that selectively co-purified with HA-BNRF1, as in Figure 2F.

(D) Immunoblot analysis of 1% input and anti-HA immunopurified GFP or SMC6 complexes from P3HR-1 untreated or treated with doxycycline (5µg/ml) and bortezomib (5nM) for 6hrs, as indicated. Representative of n=2 independent experiments.

(E) Immunoblot analysis of WCL from P3HR-1 ZHT/RHT cells induced for lytic replication in the presence of calpeptin for 24h, as indicated.

(F) Immunoblot analysis of WCL from P3HR-1 ZHT/RHT expressing the indicated sgRNAs and induced for lytic replication for 24hrs, as indicated.

(G) Immunoblot analysis of WCL from Cas9+ P3HR-1 ZHT/RHT cells expressing the indicated sgRNAs and induced for lytic replication, as indicated.

(H) Immunoblot analysis of 1% input and anti-HA immunopurified BNRF1 from P3HR-1 treated with doxycycline (5µg/ml), bortezomib (5nM), 4HT and NaB for 6hrs, as indicated. Representative of two independent experiments.

(I) Immunoblot analysis of 1% input and SMC6 complexes immunopurified from P3HR-1 that were induced into lytic cycle by 4HT/NaB and treated with bortezomib (5nM) and/or calpeptin (100µM), as indicated. Samples were blotted for poly-ubiquitin (poly-Ub) using the antibody P4D1 or for SMC6. Representative of two independent experiments.

Figure S3. Related to Figure 3: BNRF1 associates with SMC6 in nuclear puncta.

(A) Immunoblot analysis of 1% input and anti-HA immunopurified GFP or BNRF1 complexes from P3HR-1 untreated or treated with doxycycline (5µg/ml) to induce cDNA, bortezomib (5nM) for 6hrs, as indicated. Representative of two independent experiments.

(B) Immunofluorescence analysis of DAPI, doxycycline-induced HA-tagged SMC6 and stably expressed V5-tagged BNRF1 in EBV+ Akata. Cells were treated with doxycycline (5 µg/ml) and bortezomib (5 nM) for 12hrs. Representative of n=3 experiments.

(C) Zoom image of cells from S3B boxed in white.

(D) 3D reconstruction of cells as in (B). Representative of three independent experiments.

(E) Immunoblot analysis of 1% input and anti-HA immunopurified complexes from P3HR-1 that were doxycycline (5µg/ml) induced for wildtype (WT) or deletion mutant BNRF1 constructs in the presence of bortezomib (5 nM) for 6 hours. Representative of n=2 experiments.

Figure S4. Related to Figure 4: BNRF1 supports late lytic cycle progression.

(A) RNA-seq dataset principal component (PC) analysis, as in Figure 4A, of P3HR-1 cells expressing control or BNRF1 sgRNAs and uninduced or induced, as indicated.

(B) Mean ±SEM values from n=3 replicates of qRT-PCR analysis of late gene BcLF1 and BCRF1 transcripts from P3HR-1 ZHT/RHT cells with BXLF1 or BNRF1 sgRNAs induced by 4HT/NaB for 24 hours.

(C) T7-endonuclease DNA mismatch assay of P3HR-1 cells with control or BXLF1 sgRNAs. Arrows indicating mismatch cleavage products, indicative of successful EBV genomic CRISPR editing.

(D) Immunoblot analysis of WCL from Akata EBV+ cells with control or BNRF1 sgRNAs, induced into lytic cycle with anti-human IgG (15 µg/ml) as indicated, for 48hrs, representative of n=3 replicates.

(E) FACS plot of PM gp350 levels in Akata-EBV+ cells with control BXLF1 or BNRF1 sgRNAs, induced by anti-human IgG as indicated, for 48hrs.

(F) Mean ±SEM PM gp350 from n=5 replicates, as in E.

(G) Mean ±SEM qRT-PCR values from n=3 replicates of EBV intracellular genome copy number from P3HR-1 cells with BXLF1 or BNRF1 sgRNA induced into by IgG crosslinking for 48hours.

(H) FACS plots of green Raji assay analysis of infectious EBV titers produced from EBV+ Akata with BXLF1 or BNRF1 sgRNA induced by IgG crosslinking or 48 hours and then co-incubated with Raji cells.****$p < 0.0001$. ***$p<0.001$. **$p < 0.01$.

Figure S5. Related to Figure 5: BNRF1 is critical for viral replication compartment formation.

(A) Confocal immunofluorescence analysis of P3HR-1 ZHT/RHT cells with the indicated sgRNA induced for 24h with 4HT/NaB and stained for DAPI, BMRF1 or EdC. Zoomed images of cells in white boxes are shown below. Representative of n=3 replicates.

(B) Total fluorescent intensity analysis in 5 randomly selected images of cells with control BXLF1 or BNRF1 sgRNA expression, a representative panel of which is shown on the left. Shown bottom right are the average EdC fluorescence intensity ± SEM values from 5 fields.

(C) 3D reconstruction of P3HR1 ZHT/RHT control cells induced by 4HT/NaB as in (A).

(D) Confocal immunofluorescence analysis of EBV+ Akata cells expressing the indicated sgRNA and BNRF1 rescue cDNA that were induced by αIgG crosslinking for 48 h and stained for DAPI, BMRF1 or EdC. Zoomed images of cells in white boxes are shown below. Representative of n=3 replicates.

(E) Immunoblot analysis of WCL from Akata-EBV+ cells with control or BNRF1 sgRNAs induced by αIgG-crosslinking for 48h. Representative of n=2 replicates.

Figure S6. Related to Figure 5: BNRF1 counteracts RC suppression by SMC6.

(A) Confocal immunofluorescence analysis of P3HR-1 ZHT/RHT cells with the indicated sgRNA induced for 24h with 4HT/NaB and stained for DAPI, BMRF1 or EdC. Zoomed images of cells in white boxes are shown below. Representative of n=2 replicates.

(B) Immunoblot analysis of WCL from P3HR-1 ZHT/RHT cells with the indicated sgRNAs and induced for lytic replication, as indicated. Representative of n=3 replicates.

(C) Confocal immunofluorescence analysis of EBV+ Akata cells with the indicated sgRNA induced for 48h with αIgG and stained for DAPI, BMRF1 or EdC. Zoomed images of cells in white boxes are shown below. Representative of n=2 replicates.

(D) Immunoblot analysis of WCL from EBV+ Akata cells with the indicated sgRNAs and induced for lytic replication, as indicated. Representative of n=3 replicates.

(E) Mean ±SEM values of FACS analysis of % gp350+ cells from n=3 replicates of Akata cells expressing the indicated sgRNAs and mock induced or induced for lytic replication, as indicated.

(F) Mean ±SEM values of infectious EBV titers produced by EBV+ Akata with the indicated sgRNAs and induced by αIgG crosslinking or 48 hours. Data are from n=3 green Daudi assay replicates. *$p<0.05$.

(G) Immunoblot analysis of WCL from EBV+ Akata cells with the indicated sgRNAs and induced for lytic replication, as indicated. Representative of n=2 replicates.

(H) Mean ±SEM values of infectious EBV titers produced by EBV+ Akata with the indicated sgRNAs and induced by αIgG crosslinking or 48 hours. Data are from n=3 green Daudi assay replicates. ****$p < 0.0001$, ns=non-significant.

Figure S7. Related to Figure 5: multiple SMC5/6 complex components are important for RC suppression in absence of BNRF1.

(A) Immunoblot analysis of WCL from P3HR-1 ZHT/RHT with the indicated sgRNA and induced by 4HT/NaB for 24h, as indicated.

or with control, SMC5, NSE2 or NSE3 sgRNAs, chemically induced into lytic cycle for 24hrs. Representative of two independent experiments.

(B) Confocal immunofluorescence analysis of P3HR-1 ZHT/RHT cells with the indicated sgRNAs induced by 4HT/NaB for 24h and treated with bortezomib (5 nM), as indicated.

(C) Mean ±SEM values of percentages of nuclei with RC from N=3 replicates, as in B, using data from 5 randomly selected panels off 75 nuclei, using the ImageJ “Particle Analysis” plugin.

(D) Immunoblot analysis of WCL from EBV+ Akata cells with control or BNRF1/SMC5 sgRNAs, induced into lytic cycle for 48h as indicated.

(E) Immunoblot analysis of WCL from EBV+ Akata cells with control or BNRF1/NSE2 sgRNAs, induced into lytic cycle for 48h as indicated.

(F) Confocal immunofluorescence analysis of EBV+ Akata cells with the indicated sgRNAs induced by αIgG crosslinking for 48h.

(G) Mean ±SEM values of percentages of nuclei with RC from N=3 replicates, as in B, using data from 4 randomly selected panels off 80 nuclei, using the ImageJ “Particle Analysis” plugin.

Blots and images are representative of n=2 replicates. ****$p < 0.0001$, ***$p < 0.001$, **$p<0.01$.

Supplementary Table	
CRIPSR analysis	
BNRF1 sg#1 (antisense) _Forward	5’ – CGA GTA AGT GTC TCG CAG CG– 3’
BNRF1 sg#2_Forward	5’ – CTC CAC GCG AAG CAC GTA CG – 3’
BXLF1_Forward	5’ – TTG TAG TCC CTG AAC CGA TG – 3’
SMC5 sg#1_Forward	5’ – TTT ATT TCT CTC ATA CCT GA – 3’
SMC5 sg#2_Forward	5’ – CTG CAA CAG CGG CAG CTG CG – 3’
SMC6 sg#1_Forward	5’ – AAT AGC CTA ATT GAC ATG AG – 3’
SMC6 sg#2_Forward	5’ – TTT CTT ATA ACT AGG CTC CG – 3’
NSMCE2 sg#1_Forward	5’ – ATA TAG TAT GGA CAA GGC AA – 3’
NSMCE2 sg#2_Forward	5’ – GCA ACT AAA CCA TTA TGT AA – 3’
NSMCE3 sg#1_Forward	5’ – GAG ACA TGT TGC AAA AAC CG – 3’
NSMCE3 sg#2_Forward	5’ – GAG CCA TAG CGG AAA CCC CG – 3’
CAPNS1 sg#1_Forward	5’ – TCA CAG GCG GGG TTA CCG AG – 3’
CAPNS1 sg#2_Forward	5’ – CTG CAC CGA GTG GTT CCG CA – 3’
cDNA Rescue	

Genomic DNA	5’ – CGA GTA AGT GTC TCG CAG CGC GGA – 3’
Rescue cDNA_Forward	5’ – CGA GTA AGT GTC TCG CAG CGC AGA – 3’
Rescue cDNA sequence surrounding the PAM site mutation (in red, sgRNA sequence in yellow)	5’ – TGAAGGACCAAGTGGCCCGAGTAAGTGTCTCGCA GCGCAGACACGATCTTTAGCTCGTCGGC – 3’
BNRF1 mutagenesis	
BNRF1 M1 del3-300aa_Forward	5’ – GGG GAC AAC TTT GTA CAA AAA AGT TGG CAC CAT GGA AGT TAA TGC AAT AGC ATC ATC G – 3’
BNRF1 M2 del301-600aa_Forward	5’ – CAC CCC GGC CTC TTT CCC TTC TCT CCG TCT TAC GAG TTG CCC TG – 3’
BNRF1 M3 del601-900aa_Forward	5’ – ATG TGG ACG AGA GCA TGG ACA TCC AGC GGG GAG TGA CCA TCA C – 3’
BNRF1 M4 del901-1200aa_Forward	5’ – GTG GAG ATG GCC CTG GCC GGG CTG CCT TGT TGG GTG CAA GGC TC – 3’
BNRF1 M5 del1101-1312aa_Forward	5’ – GGG GAC AAC TTT GTA CAA AAA AGT TGG CAC CAT GGA AGA GAG GGG CAG G – 3’
qPCR primer sequence	
BALF5_Forward	5’ – GAG CGA TCT TGG CAA TCT CT – 3’
BALF5_Reverse	5’ – TGG TCA TGG ATC TGC TAA ACC – 3’
ChIP-qPCR primer sequence	
OrilytR_Forward	5’ – CGC TGG TTA AGC TGA CGA CCT – 3’
OrilytR_Reverse	5’ – GCC CTG GCT AGG AAA GGG AGG AA – 3’